
جامعة الملك عبدالله
للعلوم والتقنية
King Abdullah University of
Science and Technology

Composite Multiple-Mode Orthogonal Frequency Division Multiplexing with Index Modulation

Item Type	Article
Authors	Li, Jun; Dang, Shuping; Huang, Yu; Chen, Pengxu; Qi, Xiaomin; Wen, Miaowen; Arslan, Huseyin
Citation	Li, J., Dang, S., Huang, Y., Chen, P., Qi, X., Wen, M., & Arslan, H. (2022). Composite Multiple-Mode Orthogonal Frequency Division Multiplexing with Index Modulation. IEEE Transactions on Wireless Communications, 1–1. https://doi.org/10.1109/twc.2022.3220752
Eprint version	Post-print
DOI	10.1109/TWC.2022.3220752
Publisher	IEEE
Journal	IEEE Transactions on Wireless Communications
Rights	This is an accepted manuscript version of a paper before final publisher editing and formatting. Archived with thanks to IEEE. The version of record is available from IEEE Transactions on Wireless Communications.
Download date	13/04/2023 21:48:04
Link to Item	http://hdl.handle.net/10754/685605

This article has been accepted for publication in IEEE Transactions on Wireless Communications. This is the author's version which has not been fully edited and content may change prior to final publication. Citation information: DOI 10.1109/TWC.2022.3220752

Composite Multiple-Mode Orthogonal Frequency Division Multiplexing with Index Modulation

Jun Li, *Member, IEEE,* Shuping Dang, *Member, IEEE,* Yu Huang, *Member, IEEE,* Pengxu Chen, Xiaomin Qi, Miaowen Wen, *Senior Member, IEEE,* and Huseyin Arslan, *Fellow, IEEE*

***Abstract*—In this paper, we propose a composite multiple-mode orthogonal frequency division multiplexing with index modulation (C-MM-OFDM-IM) scheme to increase the spectral efficiency (SE) of OFDM-IM systems by extending the indexing to the energy and constellation domains. In C-MM-OFDM-IM, the information bits are mapped to not only the subcarrier activation patterns (SAPs) and modulation symbols, but also the energy allocation patterns (EAPs) and constellation activation patterns (CAPs). To cope with the practical situations, we propose a variant IM scheme named C-MM-OFDM-IM-II to build a new mapping rule between information bits and the increased CAPs, capable of further increasing the SE of C-MM-OFDM-IM. Upper-bounded bit error rate (BER) and lower-bounded achievable rate are both derived in closed-form to evaluate the performance of C-MM-OFDM-IM(-II). Moreover, we further propose two enhanced schemes, named generalized C-MM-OFDM-IM(-II) and C-MM-OFDM with in-phase/quadrature IM(-II), where the former jointly considers all SAPs, EAPs, CAPs and modulated symbols, while the latter expands the index implementation to the in-phase and quadrature constellation domains. Simulation results show that C-MM-OFDM-IM(-II) outperforms the conventional OFDM-IM related schemes, especially in the high signal-to-noise ratio (SNR) region, and verify the accuracy of the theoretical analysis for the upper-bounded BER and achievable rate.**

***Index Terms*—Orthogonal frequency division multiplexing (OFDM), index modulation, low-complexity detection, bit error rate (BER), achievable rate.**

I. Introduction

DUE to the rapid growth in the number of mobile users and smart devices, several novel techniques are proposed to accomplish the stringent demands of high date rate, high flexibility, high spectral efficiency (SE), and high energy efficiency (EE) for the sixth generation (6G) networks [1]. Index modulation (IM), as one of the novel modulation techniques, is proposed to achieve both high SE and high EE [2]. In IM, the pattern index(es) are utilized as an extra dimension to modulate bits for transmission, where the pattern could refer to the activation status of time slots, subcarriers, transmit antennas, receive antennas, linear block codes, angles, etc., depending on the specific context [3]–[5].

The IM paradigm was first applied to the space domain, which brings out a famous scheme named spatial modulation (SM) [6]. Unlike the conventional multiple-input multiple-output (MIMO) scheme, information bits of SM are first divided into index bits and modulation bits, where the former determine the index of a single active transmit antenna, while the latter generate one modulated symbol to be transmitted via the active transmit antenna. Note that SM has many benefits due to the activation of only a single transmit antenna, e.g., high EE, absence of inter-channel interference, and so on. Attracted by these advantages, space shift keying (SSK) is proposed to transmit only the index of the active transmit antenna [7]. Although SM and SSK achieve high EE, the SE is relatively low with respect to MIMO schemes. Therefore, generalized SM (GSM) in [8] and generalized SSK (GSSK) in [9] were proposed to improve the SE of SM and SSK systems, respectively, which allow transmitting multiple modulated symbols via multiple active transmit antennas. In [10], [11], quadrature SM (QSM) was proposed to increase the SE of SM systems by extending the modulation to the in-phase and quadrature constellation domains. On the other hand, in order to improve the performance of SM, the extension of SM to the time domain was also proposed, for instance, space-time shift keying [12], space time block coded SM [13], [14], differential SM (DSM) [15], etc. To further exploit the potential of SM, precoding SM (PSM) was put forward to modulate index bits through indices of receive antennas in [16]. Relying on the precoding technique, PSM obtains better performance than classic SM leveraging the activation status of transmit antennas. Due to this fact, several works related to PSM were proposed in [17]–[19]. In [17], generalised PSM (GPSM) was proposed to increase the SE of PSM systems by activating multiple receive antennas. Besides, the performance analysis of the multi-stream GPSM scheme was conducted in [18]. To further increase the SE, generalised pre-coding QSM (GPQSM) was proposed to merge GPSM with QSM in [19].

Recently, the IM paradigm has also been applied to the frequency domain by utilizing the indices of orthogonal frequency division multiplexing (OFDM) subcarriers to transmit

This work was supported in part by the Guangzhou Municipal Science and Technology Project under Grant 202102010416, in part by National Nature Science Foundation of China under Grants 61871190, 62272113 and 61872102, in part by the International Collaborative Research Program of Guangdong Science and Technology Department under Grant No. 2020A0505100061, in part by the Guangzhou University-The Hong Kong University of Science and Technology Joint Research Program under Grant YH202110, in part by Guangzhou Key Laboratory of Software-Defined Low Latency Network under Grant 202102100006, and in part by Innovation Training Program for College Students of Guangzhou Univeristy (Provincial) under Grant S202011078027.

Jun Li, Yu Huang, and Pengxu Chen are with Research Center of Intelligent Communication Engineering, School of Electronics and Communication Engineering, Guangzhou University, Guangzhou 510006, China (e-mail: {lijun52018, yuhuang}@gzhu.edu.cn, 1907400132@e.gzhu.edu.cn).

Shuping Dang is with Computer, Electrical and Mathematical Science and Engineering Division, King Abdullah University of Science and Technology (KAUST), Thuwal 23955-6900, Kingdom of Saudi Arabia (e-mail: shuping.dang@kaust.edu.sa).

Xiaomin Qi and Miaowen Wen are with the School of Electronic and Information Engineering, South China University of Technology, Guangzhou 510641, China (e-mail: qixiaomin_1@163.com; eemwwen@scut.edu.cn).

Huseyin Arslan is with the College of Engineering, Istanbul Medipol University, Istanbul 34810, Turkey (e-mail: huseyinarslan@medipol.edu.tr).

© 2022 IEEE. Personal use is permitted, but republication/redistribution requires IEEE permission. See https://www.ieee.org/publications/rights/index.html for more information.
Authorized licensed use limited to: KAUST. Downloaded on November 10,2022 at 05:42:06 UTC from IEEE Xplore. Restrictions apply.

This article has been accepted for publication in IEEE Transactions on Wireless Communications. This is the author's version which has not been fully edited and content may change prior to final publication. Citation information: DOI 10.1109/TWC.2022.3220752

index bits. In [20], OFDM with IM (OFDM-IM) was proposed to transmit the indices of a group of subcarriers as well as the modulated symbols via activated subcarriers. Similar to SM, information bits in OFDM-IM are also split into index bits and modulation bits, which determine the subcarrier activation pattern (SAP) and the modulated symbols, respectively. Because of this special configuration, OFDM-IM can obtain better performance than the conventional OFDM scheme. Note that different mapping rules between index bits and SAPs are possible and affect the bit error rate (BER) performance. The widely applied mapping rules include the combinatorial mapping rule [20] and the equiprobable subcarrier activation mapping rule [21]. Attracted by its merits, lots of research has been carried out to exploit the potential of OFDM-IM, e.g., fidelity improvement and SE improvement. For instance, the interleaved subcarrier grouping method was invented to improve the BER performance of OFDM-IM in [22]. Enhanced OFDM-IM was proposed to enhance the BER performance of OFDM-IM by extending the modulation to in-phase/quadrature constellation domains in [23]. It should be noted that not all SAPs are used for transmission, which restricts the BER performance of OFDM-IM. Therefore, a special constellation design was proposed to improve the BER performance of OFDM-IM by activating all SAPs for transmission in [24].

To increase the SE of OFDM-IM systems, a generalized OFDM-IM scheme was proposed to encode a large number of index bits in [25]. In [26], the authors proposed a layered OFDM-IM scheme to increase the number of index bits by selecting SAPs via multiple layers. From a different perspective, the OFDM with index and composition modulation (OFDM-ICM) was proposed in [27] to increase the SE by extending the indexing to the energy domain. In addition, OFDM-IM was further applied to the conventional MIMO system to largely increase its SE [28]. By leveraging the full set of available subcarriers, (generalized-)dual-mode IM aided OFDM ((G)DM-IM-OFDM) was proposed to utilize both selected and unselected subcarriers to transmit modulated symbols [29], [30]. In a similar manner, the authors in [31], [33] also designed the (generalized-)multiple-mode OFDM-IM ((G-)MM-OFDM-IM) scheme to transmit modulated symbols via the full set of subcarriers. To improve the SE and BER performance of DM-IM-OFDM and MM-OFDM-IM, the OFDM with maximum distance separable code (OFDM-MDS) scheme was proposed and analyzed in [34], [35], which obtains an increasing number of index bits by using the MDS code construction for distinguishable constellation sets. In addition to the theoretical research, the practical applications of OFDM-IM were investigated in recent years, e.g., for vehicle-to-vehicle communications [36], and cognitive radio networks [37]. Except for the above research works, the low-complexity detection design was also an important research direction for OFDM-IM [38]–[40].

Motivated by the advantages of the OFDM-IM, OFDM-ICM, and MM-OFDM-IM techniques, we propose a composite MM-OFDM-IM (C-MM-OFDM-IM) scheme in this paper to further increase the SE. For details, the main contributions of this paper are summarised as the following.

- In C-MM-OFDM-IM, the information bits are comprised of index bits, composition bits, mode bits, and modulation bits, where the index bits determine the subcarrier active pattern (SAP); the composition bits indicate the energy allocation pattern (EAP); the mode bits determine the constellation activation pattern (CAP); the modulation bits generate modulated symbols. A log-likelihood ratio (LLR) based low-complexity detection method is proposed to relieve the high detection complexity brought by the optimal maximum-likelihood (ML) detection for the proposed C-MM-OFDM-IM scheme. Theoretical analyses of upper bounded BER and lower bounded achievable rate of C-MM-OFDM-IM are provided, and both are derived in closed form.
- In practice, the number of distinguishable constellation sets is generally larger than the number of activated subcarriers k, say Q ($Q > k$) constellation sets. To make the best use of Q constellation sets for improving the SE of C-MM-OFDM-IM, we propose a variant scheme termed C-MM-OFDM-IM-II to enable a new mapping relationship between the increased mode bits and Q constellation sets by adopting the Q-ary coding criterion.
- With a slight increase of implementation complexity, we propose the generalized C-MM-OFDM-IM(-II) (GC-MM-OFDM-IM(-II)) scheme to increase the SE of C-MM-OFDM-IM(-II) systems by fully considering all possible SAPs, EAPs, and CAPs. In addition, by sacrificing more implementation complexity, we further propose the C-MM-OFDM with in-phase/quadrature IM(-II) (C-MM-OFDM-IQ-IM(-II)) scheme to boost the SE of C-MM-OFDM-IM(-II) systems by extending the indexing of SAP, EAP, CAP and modulated symbols to the in-phase (I-) and quadrature (Q-) domains.
- Simulation results show that the C-MM-OFDM-IM(-II) scheme obtains better error performance than the conventional OFDM-IM and OFDM-ICM schemes under the same SE. They also verify the accuracy of the theoretical BER performance analysis and show that the proposed LLR based low-complexity detection scheme for C-MM-OFDM-IM(-II) obtains the near-optimal detection performance. Additionally, the GC-MM-OFDM-IM(-II) and C-MM-OFDM-IQ-IM(-II) schemes obtain even better performance than the C-MM-OFDM-IM(-II) scheme.

The rest of this paper is organized as follows. The C-MM-OFDM-IM(-II) scheme as well as its low-complexity detection method are proposed in Section II. The BER and achievable rate of C-MM-OFDM-IM(-II) scheme are analyzed in Section III. Then, we propose two enhanced C-MM-OFDM-IM(-II) schemes in Section IV. Simulation results are presented and discussed in Section V. Finally, the paper is concluded in Section VI.

Notations: Upper and lower case boldface letters denote matrices and column vectors, respectively. The complex number field is represented by $\mathbb{C}$. $(\cdot)^T$ and $(\cdot)^H$ represent the transpose and Hermitian transpose operations with respect to the matrix enclosed, respectively. $\mathbf{I}_M$ is an $M \times M$ identity matrix. $E\{\cdot\}$ denotes the expectation operation with respect

© 2022 IEEE. Personal use is permitted, but republication/redistribution requires IEEE permission. See https://www.ieee.org/publications/rights/index.html for more information.
Authorized licensed use limited to: KAUST. Downloaded on November 10,2022 at 05:42:06 UTC from IEEE Xplore. Restrictions apply.

This article has been accepted for publication in IEEE Transactions on Wireless Communications. This is the author's version which has not been fully edited and content may change prior to final publication. Citation information: DOI 10.1109/TWC.2022.3220752

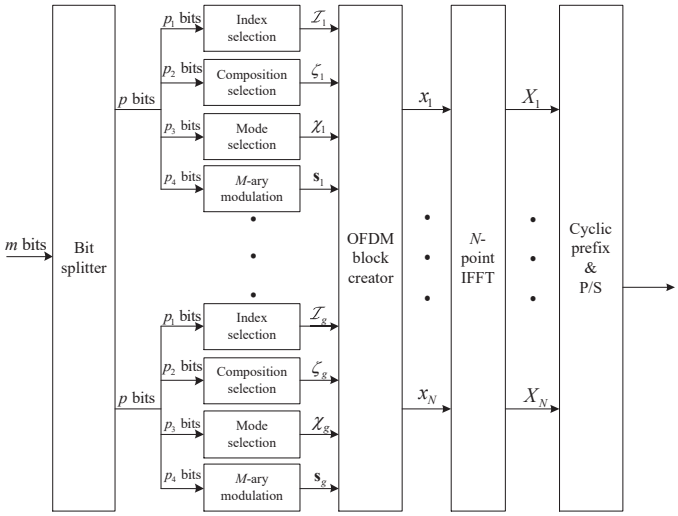


Fig. 1. System model of C-MM-OFDM-IM.

to the enclosed random variable. $||\cdot||$ denotes the Frobenius norm operation of the argument. $C(\cdot,\cdot)$ returns the binomial coefficient. $Q(\cdot)$ denotes the Gaussian Q-function. $\mathrm{diag}\{\cdot\}$ denotes a diagonal matrix whose diagonal elements are drawn from the enclosed vector. $\det\{\cdot\}$ represents the determinant of the enclosed matrix. The probability of an event is denoted by $\Pr(\cdot)$. $\lfloor\cdot\rfloor$ indicates the floor function giving the greatest integer less than or equal to the enclosed real argument. $\max(\cdot,\cdot)$ denotes the maximum operation of two arguments.

II. Proposed C-MM-OFDM-IM Scheme

In this section, we propose the C-MM-OFDM-IM scheme, which results in a larger SE than those of the OFDM-IM and OFDM-ICM schemes.

A. System Model

The system model of C-MM-OFDM-IM is depicted in Fig. 1. The same as classical OFDM and OFDM-IM schemes, N subcarriers in an OFDM block are first divided into g groups, and each group contains n subcarriers with $n = N/g$. The m incoming bits are correspondingly split into g groups, and $p = m/g$ bits are allocated to each group. Different from the conventional OFDM-ICM scheme, the p bits are now divided into four parts as $p = p_1 + p_2 + p_3 + p_4$. The first part with $p_1 = \lfloor \log_2 C(n,k) \rfloor$ bits (index bits) is used to select SAP $\mathcal{I}_\alpha = \{i_{\alpha,1}, \ldots, i_{\alpha,k}\}$ with $\{i_{\alpha,\tau}\}_{\tau=1}^{k} \in \{1,2,\ldots,n\}$. The second part with $p_2 = \lfloor \log_2 C(I-1,k-1) \rfloor$ bits (composition bits) is utilized to determine EAP $\zeta_\alpha = \{l_{\alpha,1}, \ldots, l_{\alpha,k}\}$ with $\{l_{\alpha,\iota}\}_{\iota=1}^{k} \in \{1,2,\ldots,I-1\}$. and the corresponding energy coefficients for the active subcarriers are given by $\{\sqrt{\frac{l_{\alpha,1}}{I}}, \ldots, \{\sqrt{\frac{l_{\alpha,k}}{I}}\}$. The third part with $p_3 = \lfloor \log_2(k!) \rfloor$ bits (mode bits) is utilized to determine CAP $\chi_\alpha = \{\psi_{\alpha,1}, \ldots, \psi_{\alpha,k}\}$ with $\{\psi_{\alpha,v}\}_{v=1}^{k} \in \{1,2,\ldots,k\}$ with the corresponding M-ary PSK or QAM sets $\{S_{\psi_{\alpha,1}}, \ldots, S_{\psi_{\alpha,k}}\}$, and all constellation sets should be distinguishable from each other. The last part with $p_4 = k\log_2(M)$ bits (modulation bits) is used to determine modulated symbols $\mathbf{s}_\alpha = [s_1, \ldots, s_k]$, where the modulated symbol s_v is generated from the corresponding constellation set $S_{\psi_{\alpha,v}}$, given $v \in \{1,\ldots,k\}$. Accordingly, the SE of C-MM-OFDM-IM is

$$r_{\mathrm{C-MM}} = \frac{\lfloor \log_2 C(n,k) \rfloor + \lfloor \log_2 C(I-1,k-1) \rfloor}{n} + \frac{\lfloor \log_2(k!) \rfloor + k\log_2(M)}{n}. \quad (1)$$

After obtaining SAP $\mathcal{I}_\alpha$, EAP ζ_α, CAP χ_α, and modulated symbol vector $\mathbf{s}_\alpha$, the transmitted signal vector $\mathbf{x}_\alpha$ in the frequency domain can be expressed as

$$\mathbf{x}_\alpha = [0, e_{l_{\alpha,1}} s_1, 0, e_{l_{\alpha,2}} s_2, 0, \ldots, e_{l_{\alpha,k}} s_k, 0, \ldots, 0]^T, \quad (2)$$

where $e_{l_{\alpha,\iota}} = \sqrt{\frac{l_{\alpha,\iota}}{I}}$.

For illustrative purposes, we give an example of the αth block of C-MM-OFDM-IM with $n = 4$, $k = 3$, $I = 4$ and BPSK. Assume that the three distinguishable constellation sets are given by $\{S_1 = [-1,+1], S_2 = [-(\frac{\sqrt{2}}{2} + \frac{\sqrt{2}}{2}j), (\frac{\sqrt{2}}{2} + \frac{\sqrt{2}}{2}j)], S_3 = [-j,+j]\}$. The corresponding mapping table between information bits and the transmitted vector is given in Table I. Assume that the input bits are 10000101. Based on the given mapping table, the first two bits 10 are used to select SAP $I_\alpha = [1,3,4]$. The second one bit 0 are used to select EAP $\zeta_\alpha = [1,1,2]$ with corresponding energy coefficients $[\sqrt{\frac{1}{4}}, \sqrt{\frac{1}{4}}, \sqrt{\frac{2}{4}}]$. The third two bits 00 are used to determine CAP $\chi_\alpha = [1,2,3]$. The last three bits 101 are used to generate modulated symbols $\mathbf{s}_\alpha = [+1, -(\frac{\sqrt{2}}{2} + \frac{\sqrt{2}}{2}j), +j]$. Therefore, the transmitted signal vector is finally given by

$$\mathbf{x}_\alpha = \left[\sqrt{\frac{1}{4}},\ 0,\ -\sqrt{\frac{1}{4}}\left(\frac{\sqrt{2}}{2} + \frac{\sqrt{2}}{2}j\right),\ \sqrt{\frac{2}{4}}j\right]^T = \left[\frac{1}{2},\ 0,\ -\left(\frac{\sqrt{2}}{4} + \frac{\sqrt{2}}{4}j\right),\ \frac{\sqrt{2}}{2}j\right]^T.$$

By applying the N-point IFFT to transmitted vector $\mathbf{x} = [\mathbf{x}_1^T, \ldots, \mathbf{x}_g^T]^T$, the time-domain OFDM signal can be expressed as $\mathbf{X} = [X_1, X_2, \ldots, X_N]^T$. Likewise, the OFDM signal is transmitted to the receiver after appending the CP to the beginning of $\mathbf{X}$ and completing the P/S conversion.

After propagating over multi-path fading channels, the frequency-domain received signal vector can be expressed as

$$\mathbf{y} = \mathbf{H}\mathbf{x} + \mathbf{n}, \quad (3)$$

where $\mathbf{H} = \mathrm{diag}\{\mathbf{h}\} = \mathrm{diag}\{\mathrm{h}_1, \mathrm{h}_2, \ldots, \mathrm{h}_N\}$ denotes the channel coefficient matrix whose entries follow the complex Gaussian distribution with zero mean and unit variance; $\mathbf{n}$ represents the additive Gaussian noise vector with zero mean and variance N_0. With perfect channel estimation, the transmitted signal can be estimated group by group by employing the optimal ML detection scheme as

$$\hat{\mathbf{x}}_\alpha = \arg\min_{\mathbf{x}_\alpha} \|\mathbf{y}_\alpha - \mathbf{H}_\alpha \mathbf{x}_\alpha\|^2, \quad (4)$$

where $\mathbf{H}_\alpha = \mathrm{diag}\{\mathbf{h}_\alpha\}$; $\mathbf{y}_\alpha$ and $\mathbf{h}_\alpha$ denote the αth block of $\mathbf{y}$ and $\mathbf{h}$, respectively. It can be seen from (4) that the optimal ML detection is in fact an exhaustive search over all possible candidates of the transmitted vector $\mathbf{x}_\alpha$, which results in high computational complexity, especially for large n, k, or M.

© 2022 IEEE. Personal use is permitted, but republication/redistribution requires IEEE permission. See https://www.ieee.org/publications/rights/index.html for more information.
Authorized licensed use limited to: KAUST. Downloaded on November 10,2022 at 05:42:06 UTC from IEEE Xplore. Restrictions apply.

This article has been accepted for publication in IEEE Transactions on Wireless Communications. This is the author's version which has not been fully edited and content may change prior to final publication. Citation information: DOI 10.1109/TWC.2022.3220752

TABLE I
MAPPING TABLE OF C-MM-OFDM-IM WITH $n = 4$, $k = 3$, AND $I = 4$.

SAP	EAP	CAP	Transmitted Vector	$p_1p_2p_3$	SAP	EAP	CAP	Transmitted Vector	$p_1p_2p_3$
[1, 2, 3]	[1, 1, 2]	$[S_1, S_2, S_3]$	$[e_1s_1, e_1s_2, e_2s_3, 0]$	[00000]	[1, 2, 4]	[1, 1, 2]	$[S_1, S_2, S_3]$	$[e_1s_1, e_1s_2, 0, e_2s_3]$	[01000]
		$[S_1, S_3, S_2]$	$[e_1s_1, e_1s_3, e_2s_2, 0]$	[00001]			$[S_1, S_3, S_2]$	$[e_1s_1, e_1s_3, 0, e_2s_2]$	[01001]
		$[S_2, S_1, S_3]$	$[e_1s_2, e_1s_1, e_2s_3, 0]$	[00010]			$[S_2, S_1, S_3]$	$[e_1s_2, e_1s_1, 0, e_2s_3]$	[01010]
		$[S_2, S_3, S_1]$	$[e_1s_2, e_1s_3, e_2s_1, 0]$	[00011]			$[S_2, S_3, S_1]$	$[e_1s_2, e_1s_3, 0, e_2s_1]$	[01011]
	[2, 1, 1]	$[S_1, S_2, S_3]$	$[e_2s_1, e_1s_2, e_1s_3, 0]$	[00100]		[2, 1, 1]	$[S_1, S_2, S_3]$	$[e_2s_1, e_1s_2, 0, e_1s_3]$	[01100]
		$[S_1, S_3, S_2]$	$[e_2s_1, e_1s_3, e_1s_2, 0]$	[00101]			$[S_1, S_3, S_2]$	$[e_2s_1, e_1s_3, 0, e_1s_2]$	[01101]
		$[S_2, S_1, S_3]$	$[e_2s_2, e_1s_1, e_1s_3, 0]$	[00110]			$[S_2, S_1, S_3]$	$[e_2s_2, e_1s_1, 0, e_1s_3]$	[01110]
		$[S_2, S_3, S_1]$	$[e_2s_2, e_1s_3, e_1s_1, 0]$	[00111]			$[S_2, S_3, S_1]$	$[e_2s_2, e_1s_3, 0, e_1s_1]$	[01111]
[1, 3, 4]	[1, 1, 2]	$[S_1, S_2, S_3]$	$[e_1s_1, 0, e_1s_2, e_2s_3]$	[10000]	[2, 3, 4]	[1, 1, 2]	$[S_1, S_2, S_3]$	$[0, e_1s_1, e_1s_2, e_2s_3]$	[11000]
		$[S_1, S_3, S_2]$	$[e_1s_1, 0, e_1s_3, e_2s_2]$	[10001]			$[S_1, S_3, S_2]$	$[0, e_1s_1, e_1s_3, e_2s_2]$	[11001]
		$[S_2, S_1, S_3]$	$[e_1s_2, 0, e_1s_1, e_2s_3]$	[10010]			$[S_2, S_1, S_3]$	$[0, e_1s_2, e_1s_1, e_2s_3]$	[11010]
		$[S_2, S_3, S_1]$	$[e_1s_2, 0, e_1s_3, e_2s_1]$	[10011]			$[S_2, S_3, S_1]$	$[0, e_1s_2, e_1s_3, e_2s_1]$	[11011]
	[2, 1, 1]	$[S_1, S_2, S_3]$	$[e_2s_1, 0, e_1s_2, e_1s_3]$	[10100]		[2, 1, 1]	$[S_1, S_2, S_3]$	$[0, e_2s_1, e_1s_2, e_1s_3]$	[11100]
		$[S_1, S_3, S_2]$	$[e_2s_1, 0, e_1s_3, e_1s_2]$	[10101]			$[S_1, S_3, S_2]$	$[0, e_2s_1, e_1s_3, e_1s_2]$	[11101]
		$[S_2, S_1, S_3]$	$[e_2s_2, 0, e_1s_1, e_1s_3]$	[10110]			$[S_2, S_1, S_3]$	$[0, e_2s_2, e_1s_1, e_1s_3]$	[11110]
		$[S_2, S_3, S_1]$	$[e_2s_2, 0, e_1s_3, e_1s_1]$	[10111]			$[S_2, S_3, S_1]$	$[0, e_2s_2, e_1s_3, e_1s_1]$	[11111]

* $e_1 = \sqrt{\frac{1}{4}}$, $e_2 = \sqrt{\frac{2}{4}}$

B. Low-Complexity Detection

In this subsection, we propose an LLR detection method, which largely reduces the computational complexity of the detection of the proposed C-MM-OFDM-IM scheme. For simplicity, we drop notation α in the following. The detection metric can be formulated as

$$L(\eta) = \ln \frac{\Pr(\mathrm{A}_\eta | y(\eta))}{\Pr(\bar{\mathrm{A}}_\eta | y(\eta))} = \ln \frac{\Pr(\mathrm{A}_\eta) f(y(\eta)|\mathrm{A}_\eta)}{\Pr(\bar{\mathrm{A}}_\eta) f(y(\eta)|\bar{\mathrm{A}}_\eta)}, \quad (5)$$

where $y(\eta)$ denotes the ηth element of $\mathbf{y}_\alpha$, A_η denotes the event that the ηth subcarrier is active with probability $\Pr(\mathrm{A}_\eta) = k/n$, while $\bar{\mathrm{A}}_\eta$ represents the complementary event of A_η with probability $\Pr(\bar{\mathrm{A}}_\eta) = (n-k)/n$. The conditional probability density function (PDF) $f(y(\eta)|\mathrm{A}_\eta)$ can be explicitly expressed as

$$f(y(\eta)|\mathrm{A}_\eta) = \begin{cases} \frac{1}{\pi N_0} \exp(-\frac{1}{N_0}|y(\eta) - h_\eta \hat{s}(\eta)|^2), & \eta \in \mathcal{I}, \\ \frac{1}{\pi N_0} \exp(-\frac{1}{N_0}|y(\eta)|^2), & \eta \notin \mathcal{I}. \end{cases} \quad (6)$$

By calculating all values of $L(\eta)$, $\eta = 1, \ldots, n$, we can obtain the LLR vector:

$$\mathbf{L} = [L(1), \ldots, L(n)].$$

It can be seen from (5) that the ηth subcarrier is more likely to be activated with a larger value of $L(\eta)$. In order to estimate the possible SAP, and the corresponding EAP, CAP and modulated symbols, we first sort the values of $\mathbf{L}$ as $[z_1, \ldots, z_n] = \mathrm{sort}_1([L(1), \ldots, L(n)])$, where $\mathrm{sort}_1(\cdot)$ denotes the ordering function that reorders the elements in descending order, and z_1 (z_n) denotes the position of the maximal (minimal) value in $\mathbf{L}$. Therefore, the SAP can be estimated as

$$\hat{\mathcal{I}} = [g_1, g_2, \ldots, g_k] = \mathrm{sort}_2([z_1, z_2, \ldots, z_k]), \quad (7)$$

where $\mathrm{sort}_2(\cdot)$ denotes another ordering function that reorders the elements in ascending order, and g_1 (g_k) denotes the position of the minimal (maximal) value. After obtaining estimated SAP $\hat{\mathcal{I}}$, EAP, CAP, and modulated symbols can be estimated by the following four steps:

- Sort the channels of the k subcarriers in $\hat{\mathcal{I}}$ according to the absolute values of their coefficients in decreasing order as $[\gamma_1, \ldots, \gamma_k] = \mathrm{sort}_1([|h(g_1)|^2, \ldots, |h(g_k)|^2])$.
- Estimate the EAP and CAP carried on the k subcarriers by following the order dictated in $[h(g_{\gamma_1}), \ldots, h(g_{\gamma_k})]$. Specifically, we start with the g_{γ_1}th subcarrier and estimate corresponding energy coefficient $\hat{l}_{\gamma_1}$, constellation set $S_{\hat{\psi}_{\gamma_1}}$ and transmitted symbol by $[\hat{l}_{\gamma_1}, S_{\hat{\psi}_{\gamma_1}}, \hat{s}_{\gamma_1}] = \arg\min_x |y(g_{\gamma_1}) - h(g_{\gamma_1})x|^2$. Note that x is generated by $x = \sqrt{\frac{l_{\gamma_1}}{I}} s_{\gamma_1}$, where $l_{\gamma_1} \in \{\zeta^1, \ldots, \zeta^U\}$, and $s_{\gamma_1} \in \{S_1, \ldots, S_k\}$.
- For the g_{γ_2}th subcarrier, estimate corresponding energy coefficient $\hat{l}_{\gamma_2}$, constellation set $S_{\hat{\psi}_{\gamma_2}}$, and transmitted symbol by $[\hat{l}_{\gamma_2}, S_{\hat{\psi}_{\gamma_2}}, \hat{s}_{\gamma_2}] = \arg\min_x |y(g_{\gamma_2}) - h(g_{\gamma_2})x|^2$. Unlike the first step for the g_{γ_1}th subcarrier, the estimated signal x here should be generated by eliminating the illegitimate EAPs and CAPs, which is thus given by $x = \sqrt{\frac{l_{\gamma_2}}{I}} s_{\gamma_2}$ with $l_{\gamma_2} \in \{\zeta^{leg}\}$, and $s_{\gamma_2} \in \{S_1, \ldots, S_k\} \backslash S_{\hat{\psi}_{\gamma_1}}$. It is worth noting that ζ^{leg} denotes the legitimate EAP set, which contains energy coefficient $\hat{l}_{\gamma_1}$ in the γ_1th position.
- Repeat the above process until the g_{γ_k}th subcarrier has been processed, and finally obtain corresponding energy coefficients $\{\hat{l}_{\gamma_i}\}_{i=1}^k$, constellation sets $\{S_{\hat{\psi}_{\gamma_i}}\}_{i=1}^k$, and transmitted signals $\{\hat{s}_{\gamma_i}\}_{i=1}^k$, which further result in estimated EAP $\hat{\zeta}$, estimated CAP $\hat{\chi}$, and estimated signal vector $\hat{\mathbf{s}}$.

With $\hat{I}$, $\hat{\zeta}$, $\hat{\chi}$ and $\hat{\mathbf{s}}$, the transmitted information bits can be retrieved by standard demapping and demodulation processes.

To be explicit, the estimation process for EAP and CAP is exemplified in Fig. 2 with $n = 4$, $k = 3$, and $I = 5$. Assume that the estimated SAP obtained from (7) is $\hat{\mathcal{I}} = [2, 3, 4]$, and

© 2022 IEEE. Personal use is permitted, but republication/redistribution requires IEEE permission. See https://www.ieee.org/publications/rights/index.html for more information.
Authorized licensed use limited to: KAUST. Downloaded on November 10,2022 at 05:42:06 UTC from IEEE Xplore. Restrictions apply.

This article has been accepted for publication in IEEE Transactions on Wireless Communications. This is the author's version which has not been fully edited and content may change prior to final publication. Citation information: DOI 10.1109/TWC.2022.3220752

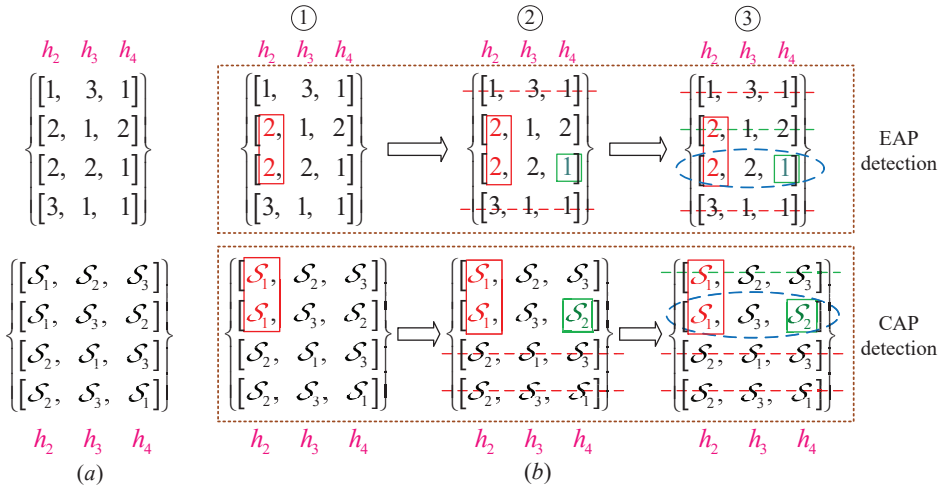


Fig. 2. Estimation process for EAP and CAP by the low-complexity detection scheme proposed in this paper.

the corresponding channels are sorted as $|h_2|^2 > |h_4|^2 > |h_3|^2$. Specifically, we first estimate energy coefficient $\hat{l}_1$, constellation set $S_{\hat{\psi}_1}$ and modulated symbol $\hat{s}_1$ for the second subcarrier h_2 via $[\hat{l}_1, S_{\hat{\psi}_1}, \hat{s}_1] = \arg\min_x |y(2) - h(2)x|^2$, where $x = \sqrt{\frac{l_1}{5}} s_1$ with $l_1 \in \{1,2,3\}$ and $s_1 \in \{S_1, S_2, S_3\}$. As shown in Fig. 2(b) that the estimation results for the second subcarrier are listed as $\hat{l}_1 = 2$ and $S_{\hat{\psi}_1} = S_1$ ($\hat{s}_1 \in S_1$). In the second step, we subsequently estimate energy coefficient $\hat{l}_3$, constellation set $S_{\hat{\psi}_3}$ and modulated symbol $\hat{s}_3$ for the fourth subcarrier h_4 via $[\hat{l}_3, S_{\hat{\psi}_3}, \hat{s}_3] = \arg\min_x |y(4) - h(4)x|^2$, where $x = \sqrt{\frac{l_3}{5}} s_3$ with $l_3 \in \{1,2\}$ and $s_3 \in \{S_2, S_3\}$. Note that the the possible energy coefficient for $\hat{l}_3$ is only selected from $\{1,2\}$ due to the first estimation $\hat{l}_1 = 2$ (see Fig. 2(b)). Similarly, the possible modulated symbol should be selected from $\{S_2, S_3\}$ due to $\hat{s}_1 \in S_1$. As also shown in Fig. 2(b) that we hereby obtain $\hat{l}_3 = 1$ and $S_{\hat{\psi}_3} = S_2$ ($\hat{s}_3 \in S_2$). In the last step for the third subcarrier h_3, we can easily find that the energy coefficient and the constellation set are straightforwardly obtained by $\hat{l}_2 = 2$ and $S_{\hat{\psi}_2} = S_3$, respectively. To further estimate the modulated symbol, we simply implement the detection criterion given by $\hat{s}_3 = \arg\min_{s \in S_3} |y(3) - h(3)s|^2$. After finishing the entire estimation process, the estimated EAP and CAP are finally obtained by $\hat{\zeta} = \{2,2,1\}$ and $\hat{\chi} = \{1,3,2\}$, respectively. It is worth noting that the estimated symbols $\hat{\mathbf{s}} = [\hat{s}_1, \ldots, \hat{s}_k]$ have already been obtained in the above estimation process.

C. Variant C-MM-OFDM-IM

In C-MM-OFDM-IM, the number of distinguishable constellation sets is equal to the number of active subcarriers k, which thereby generates $k!$ possible CAPs with the number of mode bits $p_3 = \lfloor \log_2(k!) \rfloor$. For encoding information, only 2^{p_3} CAPs are utilized, while the remaining $(k! - 2^{p_3})$ CAPs are discarded, which degrades the SE of C-MM-OFDM-IM. On the other hand, the number of distinguishable constellation sets of practical communication systems could be more than k, say Q distinguishable constellation sets with $Q > k$. In this situation, only selecting k constellation sets for transmission is a considerable waste of frequency resource.

Therefore, to fully utilize all Q distinguishable constellation sets, we proposed a variant C-MM-OFDM-IM scheme to reconstruct the mapping relationship between the mode bits and corresponding CAPs with Q constellation sets, which leads to a higher number of mode bits p_3 for obtaining an even higher SE. For the sake of distinction, we refer to the C-MM-OFDM-IM scheme with Q distinguishable constellation sets as C-MM-OFDM-IM-II in the following. Specifically, we first generate the Q-ary code as $\{\vartheta_1, \ldots, \vartheta_k\}$ by following the "$(\vartheta_1 + \ldots + \vartheta_k) \bmod Q = 0$" rue [41], where $\vartheta_v \in \{0,1,\ldots,Q-1\}$ with $v \in \{1,\ldots,k\}$. After obtaining all possible Q-ary codes, the corresponding CAPs are constructed as $\{\vartheta_1 + 1, \ldots, \vartheta_k + 1\}$. The total number of Q-ary codes is Q^{k-1}, and the number of corresponding mode bits is given by $p_3 = \lfloor \log_2(Q^{k-1}) \rfloor$. It is worth noting that $Q^{(k-1)} \geq k!$, and $Q^{(k-1)} = k!$ holds only when $Q = k = 2$. Explicitly, the SE of C-MM-OFDM-IM-II is

$$r_{\text{C-MM-II}} = \frac{\lfloor \log_2 C(n,k) \rfloor + \lfloor \log_2 C(I-1,k-1) \rfloor}{n} + \frac{+\lfloor \log_2(Q^{k-1}) \rfloor + k \log_2(M)}{n}. \quad (8)$$

As an example, we provide the quantitative comparison of the number of mode bits for C-MM-OFDM-IM and C-MM-OFDM-IM-II with $k = 3$ and $Q = 3,4$ given in Table II, Table III and Table IV. It can be seen from Table II that C-MM-OFDM-IM with $k = 3$ has 2 mode bits by selecting four legitimate CAPs (two illegitimate CAPs are unused). In C-MM-OFDM-IM-II with $Q = k = 3$, we can see from Table III that 3 mode bits are encoded benefiting from the Q-ary code construction, and there is only one unused constellation set. Keep increasing to $Q = 4$, C-MM-OFDM-IM-II with $Q = 4$ and $k = 3$ is capable of encoding 4 mode bits ($p_3 = 4$) to fully utilize all possible CAPs as shown in Table IV. It is evident that C-MM-OFDM-IM-II is able to achieve a higher SE than that of C-MM-OFDM-IM by properly designing the Q-ary code.

© 2022 IEEE. Personal use is permitted, but republication/redistribution requires IEEE permission. See https://www.ieee.org/publications/rights/index.html for more information.
Authorized licensed use limited to: KAUST. Downloaded on November 10,2022 at 05:42:06 UTC from IEEE Xplore. Restrictions apply.

This article has been accepted for publication in IEEE Transactions on Wireless Communications. This is the author's version which has not been fully edited and content may change prior to final publication. Citation information: DOI 10.1109/TWC.2022.3220752

TABLE II
MAPPING TABLE FOR C-MM-OFDM-IM WITH $k = 3$.

mode bits (p_3)	CAP
[00]	$\{1, 2, 3\}$
[01]	$\{1, 3, 2\}$
[10]	$\{2, 1, 3\}$
[11]	$\{2, 3, 1\}$
Unused	$\{3, 1, 2\}$
Unused	$\{3, 2, 1\}$

TABLE III
MAPPING TABLE FOR C-MM-OFDM-IM-II WITH $Q = k = 3$.

mode bits (p_3)	code	CAP
[000]	$\{0, 0, 0\}$	$\{1, 1, 1\}$
[001]	$\{0, 1, 2\}$	$\{1, 2, 3\}$
[010]	$\{0, 2, 1\}$	$\{1, 3, 2\}$
[011]	$\{1, 0, 2\}$	$\{2, 1, 3\}$
[100]	$\{1, 1, 1\}$	$\{2, 2, 2\}$
[101]	$\{1, 2, 0\}$	$\{2, 3, 1\}$
[110]	$\{2, 0, 1\}$	$\{3, 1, 2\}$
[111]	$\{2, 1, 0\}$	$\{3, 2, 1\}$
Unused	$\{2, 2, 2\}$	$\{3, 3, 3\}$

TABLE IV
MAPPING TABLE FOR C-MM-OFDM-IM-II WITH $k = 3$, AND $Q = 4$.

mode bits (p_3)	code	CAP	mode bits (p_3)	code	CAP
[0000]	$\{0, 0, 0\}$	$\{1, 1, 1\}$	[1000]	$\{2, 0, 2\}$	$\{3, 1, 3\}$
[0001]	$\{0, 1, 3\}$	$\{1, 2, 4\}$	[1001]	$\{2, 1, 1\}$	$\{3, 2, 2\}$
[0010]	$\{0, 2, 2\}$	$\{1, 3, 3\}$	[1010]	$\{2, 2, 0\}$	$\{3, 3, 1\}$
[0011]	$\{0, 3, 1\}$	$\{1, 4, 2\}$	[1011]	$\{2, 3, 3\}$	$\{3, 4, 4\}$
[0100]	$\{1, 0, 3\}$	$\{2, 1, 4\}$	[1100]	$\{3, 0, 1\}$	$\{4, 1, 2\}$
[0101]	$\{1, 1, 2\}$	$\{2, 2, 3\}$	[1101]	$\{3, 1, 0\}$	$\{4, 2, 1\}$
[0110]	$\{1, 2, 1\}$	$\{2, 3, 2\}$	[1110]	$\{3, 2, 3\}$	$\{4, 3, 4\}$
[0111]	$\{1, 3, 0\}$	$\{2, 4, 1\}$	[1111]	$\{3, 3, 2\}$	$\{4, 4, 3\}$

TABLE V
MULTIPLICATION COMPARISON OF DETECTION METHODS FOR C-MM-OFDM-IM(-II).

	Proposed method	ML	Reduction (%)
($n = 4$, $k = 2$, $I = 4$, BPSK)	92	512	82%
($n = 4$, $k = 2$, $I = 5$, $Q = 4$, QPSK)	136	8192	98%
($n = 8$, $k = 3$, $I = 8$, BPSK)	164	262114	99%

D. Complexity Analysis

To explicitly show the computing advantage of the low-complexity detection method, we quantify the computational complexity of the low-complexity and optimal ML detections based on the number of complex multiplications for C-MM-OFDM-IM(-II).

In C-MM-OFDM-IM, the computational complexity of the proposed detection method stems from the calculation of LLR values $\{L(\eta)\}_{\eta=1}^{n}$ in (5), and the estimations of EAP and CAP. Specifically, calculating $f(y(\eta)|\mathrm{A}_\eta)$, $f(y(\eta)|\bar{\mathrm{A}}_\eta)$ and $\Pr(\mathrm{A}_\eta)$ needs $(2M + 12)$ multiplications for a given η. Therefore, obtaining $\{L(\eta)\}_{\eta=1}^{n}$ requires $n(2M + 12)$ multiplications. In addition, estimating EAP and SAP needs $kM(k+1)$ multiplications ($kM(2Q-k+1)$ for C-MM-OFDM-IM-II). Therefore, the total number of multiplications for the proposed detection in C-MM-OFDM-IM is $(Mk^2 + 2Mn + 12n + kM)$. On the other hand, the total numbers of complex multiplications of ML detection for C-MM-OFDM-IM and C-MM-OFDM-IM-II are given by $n2^{nr_{\mathrm{C-MM}}+1}$ and $n2^{nr_{\mathrm{C-MM-II}}+1}$, respectively. Note that the computational complexity of the ML detection for traditional OFDM is $2nM$, which is even less than that of the low-complexity detection for C-MM-OFDM-IM(-II). However, as will be verified in Section V, C-MM-OFDM-IM(-II) outperforms OFDM with a considerable performance gain, which indicates a worthwhile compromise of detection complexity for communication performance.

For better illustration, we present the computational complexity comparison of the low-complexity and ML detections for C-MM-OFDM-IM(-II) in Table V. To be specific, the ML detection requires 512 multiplications while the low-complexity detection only needs 92 multiplications, which achieves a 77% complexity reduction for C-MM-OFDM-IM with $n = 4$, $k = 2$, $I = 4$, and BPSK. For C-MM-OFDM-IM-II with $n = 4$, $k = 2$, $I = 5$, $Q = 4$, and BPSK, the low-complexity detection attains up to a 98% complexity reduction. Moreover, a 99% complexity reduction can even be obtained by the proposed detection for C-MM-OFDM-IM with $n = 8$, $k = 3$, $I = 8$, and BPSK. According to results shown in this table, we can confirm that the low-complexity detection is able to considerably reduce the detection complexity, especially for large values of n and M.

© 2022 IEEE. Personal use is permitted, but republication/redistribution requires IEEE permission. See https://www.ieee.org/publications/rights/index.html for more information.
Authorized licensed use limited to: KAUST. Downloaded on November 10,2022 at 05:42:06 UTC from IEEE Xplore. Restrictions apply.

This article has been accepted for publication in IEEE Transactions on Wireless Communications. This is the author's version which has not been fully edited and content may change prior to final publication. Citation information: DOI 10.1109/TWC.2022.3220752

III. Performance Analysis

A. Analysis of the Upper Bound on BER

In this subsection, we theoretically deduce the upper bound on the BER of C-MM-OFDM-IM(-II) assuming the perfect channel state information (CSI) at the receiver. According to (4), the conditional pairwise error probability (PEP) on $\mathbf{H}_\alpha$ is given by

$$\begin{aligned}&\Pr\left\{\mathbf{x}_\alpha \to \hat{\mathbf{x}}_\alpha|\mathbf{H}_\alpha\right\}\\ =&\Pr\left\{\|\mathbf{y}_\alpha-\mathbf{H}_\alpha\mathbf{x}_\alpha\|^2>\|\mathbf{y}_\alpha-\mathbf{H}_\alpha\hat{\mathbf{x}}_\alpha\|^2\right\}\\ =&Q\left(\sqrt{\frac{\|\mathbf{H}_\alpha(\mathbf{x}_\alpha-\hat{\mathbf{x}}_\alpha)\|^2}{2N_0}}\right).\end{aligned} \tag{9}$$

Applying the Q-function approximation $Q(x)\cong\frac{1}{12}e^{-\frac{x^2}{2}}+\frac{1}{4}e^{-\frac{2x^2}{3}}$ derived in [42], the unconditional PEP can be approximated as

$$\begin{aligned}&\Pr\left\{\mathbf{x}_\alpha \to \hat{\mathbf{x}}_\alpha\right\}=E_{\mathbf{H}_\alpha}\left\{\Pr\left\{\mathbf{x}_\alpha \to \hat{\mathbf{x}}_\alpha|\mathbf{H}_\alpha\right\}\right\}\\ &=\frac{1/12}{(\det(\mathbf{I}_N+q_1\mathbf{K}\mathbf{A}))}+\frac{1/4}{(\det(\mathbf{I}_N+q_2\mathbf{K}\mathbf{A}))},\end{aligned} \tag{10}$$

where $\mathbf{A}=\mathrm{diag}\{\mathbf{x}_\alpha-\hat{\mathbf{x}}_\alpha\}^H\mathrm{diag}\{\mathbf{x}_\alpha-\hat{\mathbf{x}}_\alpha\}$; $\mathbf{K}=E\{\mathbf{H}_\alpha\mathbf{H}_\alpha^H\}$ is the covariance matrix of $\mathbf{H}_\alpha$; $q_1=1/(2N_0)$ and $q_2=2/(3N_0)$. Having obtained the unconditional PEP in (10), an upper bound on BER can be derived according to the union bounding technique as [43]

$$P_e\le\frac{1}{p2^p}\sum_{\mathbf{x}_\alpha}\sum_{\hat{\mathbf{x}}_\alpha\neq\mathbf{x}_\alpha}d(\mathbf{x}_\alpha\to\hat{\mathbf{x}}_\alpha)\Pr\left\{\mathbf{x}_\alpha\to\hat{\mathbf{x}}_\alpha\right\}, \tag{11}$$

where $d(\mathbf{x}_\alpha\to\hat{\mathbf{x}}_\alpha)$ measures the number of bits in error between $\mathbf{x}_\alpha$ and $\hat{\mathbf{x}}_\alpha$.

B. Analysis of Achievable Rate

We derive the achievable rate of the proposed C-MM-OFDM-IM(-II) system according to the definition of mutual information between $\mathbf{y}_\alpha$ and $\mathbf{x}_\alpha$, which is given by [44]

$$\begin{aligned}R=\frac{1}{n}I(\mathbf{x}_\alpha;\mathbf{y}_\alpha)&=\frac{1}{n}\left(H(\mathbf{x})-H(\mathbf{x}|\mathbf{y})\right)\\ &=\frac{p}{n}-\frac{1}{n}E_{\mathbf{h}_\alpha}\left[H(\mathbf{x}_\alpha|\mathbf{y}_\alpha,\mathbf{h}_\alpha)\right].\end{aligned} \tag{12}$$

The conditional PDF of $\mathbf{y}_\alpha$ on $\mathbf{x}_\alpha$ and $\mathbf{h}_\alpha$ is given by

$$f(\mathbf{y}_\alpha|\mathbf{x}_\alpha,\mathbf{h}_\alpha)=\frac{1}{(\pi N_0)^n}\exp(||\mathbf{y}_\alpha-\mathrm{diag}\{\mathbf{h}_\alpha\}\mathbf{x}_\alpha||^2), \tag{13}$$

and that solely on $\mathbf{h}_\alpha$ is determined by

$$f(\mathbf{y}_\alpha|\mathbf{h}_\alpha)=\frac{1}{2^p}\sum_{\varsigma=1}^{2^p}f(\mathbf{y}_\alpha|\mathbf{x}_\alpha^\varsigma,\mathbf{h}_\alpha), \tag{14}$$

where $\mathbf{x}_\alpha^\varsigma$ denotes the ςth observation of $\mathbf{x}_\alpha$. By scrutinizing (13) and (14), unfortunately, we find no closed form solution to the expression given in (12). Therefore, we resort to the lower-bounded technique proposed in [44] to obtain a lower bound on the achievable rate as

$$\begin{aligned}r\ge&\frac{p}{n}-(\log_2(e)-1)\\ &-\frac{1}{n2^p}\sum_{\varpi=1}^{2^p}\left(\log_2\sum_{\varsigma=1}^{2^p}\frac{1}{\det(\mathbf{I}_N+\Xi_{\varpi,\varsigma})}\right),\end{aligned} \tag{15}$$

where $\Xi_{\varpi,\varsigma}=\frac{1}{2N_0}\mathrm{diag}\{\mathbf{x}_\alpha^\varpi-\mathbf{x}_\alpha^\varsigma\}^H\mathrm{diag}\{\mathbf{x}_\alpha^\varpi-\mathbf{x}_\alpha^\varsigma\}$.

IV. Enhanced C-MM-OFDM-IM Scheme

In C-MM-OFDM-IM(-II), only 2^{p_1} SAPs are used for transmission with p_1 index bits, and, therefore, $(\log_2 C(n,k)-2^{p_1})$ SAPs are not adopted. The same inefficient situation might apply to generating p_2 composition bits and p_3 mode bits. Therefore, in this section, we propose two enhanced C-MM-OFDM-IM(-II) schemes, named GC-MM-OFDM-IM(-II) and C-MM-OFDM-IQ-IM(-II), to increase the SE of C-MM-OFDM-IM(-II) by fully exploiting all available SAPs, EAPs, and CAPs.

A. GC-MM-OFDM-IM

In GC-MM-OFDM-IM, we fully utilize all $C(n,k)$ SAPs, $C(I-1,k-1)$ EAPs, and $k!$ CAPs to construct all possible transmitted signal vectors. As a result, the number of all possible transmitted signal vectors is given by $(C(n,k)\times C(I-1,k-1)\times k!\times M^k)$, and the corresponding SE of GC-MM-OFDM-IM is then calculated by

$$r_{\mathrm{GC-MM}}=\frac{\lfloor\log_2(C(n,k)\times C(I-1,k-1)\times k!\times M^k)\rfloor}{n}. \tag{16}$$

Similarly, the number of all possible transmitted signal vectors for G-MM-OFDM-IM-II is given by $(C(n,k)\times C(I-1,k-1)\times Q^{k-1}\times M^k)$, and the corresponding SE of GC-MM-OFDM-IM-II is likewise calculated by

$$r_{\mathrm{GC-MM-II}}=\frac{\lfloor\log_2(C(n,k)\times C(I-1,k-1)\times Q^{k-1}\times M^k)\rfloor}{n}. \tag{17}$$

Observing from the above derived SE relations, it is surprising that by properly designing the parameters of n, k, I, and Q, the SE of GC-MM-OFDM-IM(-II) can be considerably increased without investing any additional frequency and spatial resource.

For the purpose of illustration, we provide an example for GC-MM-OFDM-IM(-II) in Table VI. Let us first examine the SE comparisons of OFDM-ICM, C-MM-OFDM-IM(-II) and GC-MM-OFDM-IM(-II) with $n=4$. Specifically, for the case with $n=4$, $k=2$, $M=2$, $I=4$, and $Q=2$, C-MM-OFDM-IM obtains the same SE of 1.5 bps/Hz as C-MM-OFDM-IM-II with $Q=K=2$, and both two schemes achieve higher SEs than OFDM-ICM. Besides, GC-MM-OFDM-IM(-II) obtains a higher SE than C-MM-OFDM-IM(-II). By increasing Q up to 4 while keeping all the other settings exactly the same as $n=4$, $k=2$, $M=2$, and $I=4$, C-MM-OFDM-IM-II with 1.75 bps/Hz achieves a higher SE than C-MM-OFDM-IM with 1.5 bps/Hz, which verifies the SE advantage of C-MM-OFDM-IM-II detailed in Section II. In this case, GC-MM-OFDM-IM(-II) still maintains a higher SE than C-MM-OFDM-IM(-II). However, GC-MM-OFDM-IM(-II) is not always better than C-MM-OFDM-IM(-II) in terms of SE. For example, when $n=4$, $k=3$, $M=2$, $I=4$, and $Q=4$, although GC-MM-OFDM-IM with 2.25 bps/Hz has a higher SE than C-MM-OFDM-IM with 2 bps/Hz, GC-MM-OFDM-IM-II obtains the same SE as C-MM-OFDM-IM-II both with 2.5 bps/Hz. For another case with $n=4$, $k=3$, $M=4$, $I=3$, and $Q=4$, GC-MM-OFDM-IM(-II) attains exactly the same SE of 2.5 bps/Hz (3

© 2022 IEEE. Personal use is permitted, but republication/redistribution requires IEEE permission. See https://www.ieee.org/publications/rights/index.html for more information.
Authorized licensed use limited to: KAUST. Downloaded on November 10,2022 at 05:42:06 UTC from IEEE Xplore. Restrictions apply.

This article has been accepted for publication in IEEE Transactions on Wireless Communications. This is the author's version which has not been fully edited and content may change prior to final publication. Citation information: DOI 10.1109/TWC.2022.3220752

TABLE VI
SE COMPARISON (BPS/HZ) AMONG DIFFERENT CONFIGURATIONS WITH $n = 4$ AND $n = 8$.

(n, k, M, I, Q)	ICM	C-MM-IM	GC-MM-IM	C-MM-IM-II	GC-MM-IM-II
(4, 2, 2, 4, 2)	1.25	1.5	1.75	1.5	1.75
(4, 2, 2, 4, 4)	1.25	1.5	1.75	1.75	2
(4, 3, 2, 4, 4)	1.5	2	2.25	2.5	2.5
(4, 3, 4, 3, 4)	2	2.5	2.5	3	3
(8, 2, 2, 4, 2)	0.875	1	1.125	1	1.125
(8, 3, 2, 4, 4)	1.125	1.375	1.5	1.625	1.75
(8, 3, 2, 6, 8)	1.375	1.625	1.75	2.125	2.25
(8, 4, 4, 6, 6)	2.125	2.625	2.75	3	3.125

bps/Hz) as C-MM-OFDM-IM(-II). It is worth noting that all C-MM-OFDM-IM(-II) and GC-MM-OFDM-IM(-II) schemes achieve higher SEs than the conventional OFDM-ICM, and GC-MM-OFDM-IM(-II) is even able to obtain a higher SE than C-MM-OFDM-IM(-II) by properly designing n, k, M, I, and Q.

To further validate the performance advantage of the proposed enhanced schemes, we investigate more configurations for GC-MM-OFDM-IM(-II) with $n = 8$. To be specific, it can be seen from Table VI that (G)C-MM-OFDM-IM and (G)C-MM-OFDM-IM-II under the setup of $n = 8$, $k = 2$, $M = 2$, $I = 4$, and $Q = 2$ have the same SE of 1 bps/Hz (1.125 bps/Hz) because of $Q = K = 2$, and GC-MM-OFDM-IM(-II) obtains a higher SE than C-MM-OFDM-IM(-II). For $Q = 4$ while maintaining $n = 8$, $k = 3$, $M = 2$, $I = 4$, and $Q = 4$, we also find that (G)C-MM-OFDM-IM-II has a higher SE than (G)C-MM-OFDM-IM-II, and GC-MM-OFDM-IM(-II) obtains the larger SE than C-MM-OFDM-IM(-II). Under the configuration of $n = 8$, $k = \{3, 4\}$, $M = \{2, 4\}$, $I = 6$, $Q = \{6, 8\}$, we still obtain the consistent results that GC-MM-OFDM-IM(-II) achieves an SE performance gain over C-MM-OFDM-IM(-II). Therefore, we can summarize from above results that our proposed (G)C-MM-OFDM-IM(-II) scheme achieves a higher SE than the conventional OFDM-ICM scheme, and GC-MM-OFDM-IM(-II) is even able to obtain the a higher SE than C-MM-OFDM-IM(-II) by properly configuring the system parameters.

B. C-MM-OFDM-IQ-IM

The second enhanced C-MM-OFDM-IM scheme is called C-MM-OFDM-IQ-IM(-II), which selects the SAP, EAP, CAP and modulated symbols from the in-phase and quadrature constellation domains for indexing to greatly increase the SE of C-MM-OFDM-IM(-II). For simplicity, we use two orthogonal pulse amplitude modulation (PAM) constellations for the purpose of demonstration which is composed of the real and imaginary parts of the modulated symbols in the in-phase and quadrature constellation domains.

In C-MM-OFDM-IQ-IM, to facilitate independent coding and processing in both in-phase and quadrature constellation domains, a total number of p_t information bits are first divided into two parts, i.e., I-part with p^I bits and Q-part with p^Q bits. For the I-part with p^I bits, k among n subcarriers are activated for transmitting the real part of the transmitted signal. Specifically, p^I bits are also split into four parts as $p^I = p_1^I + p_2^I + p_3^I + p_4^I$. The $p_1^I = \lfloor \log_2 C(n,k) \rfloor$ bits (index bits) are used to select SAP $\mathcal{I}^I = \{i_1^I, \ldots, i_k^I\}$ with $\{i_\tau^I\}_{\tau=1}^k \in \{1, 2, \ldots, n\}$. The $p_2^I = \lfloor \log_2 C(I-1, k-1) \rfloor$ bits (composition bits) are utilized to determine EAP $\zeta^I = \{l_1^I, \ldots, l_k^I\}$ with $\{l_\iota^I\}_{\iota=1}^k \in \{1, 2, \ldots, I-1\}$ and $l_1^I + \cdots + l_k^I = I$. Note that the corresponding energy coefficients for the active subcarriers in the I-part are given by $\{\sqrt{\frac{l_1^I}{I}}, \ldots, \{\sqrt{\frac{l_k^I}{I}}\}$. The $p_3^I = \lfloor \log_2(k!) \rfloor$ bits (mode bits) are utilized to determine CAP $\chi^I = \{\psi_1^I, \ldots, \psi_k^I\}$ with $\{\psi_v^I\}_{v=1}^k \in \{1, 2, \ldots, k\}$ according to the M^I-ary PAM set $\{S_{\psi_1}^I, \ldots, S_{\psi_k}^I\}$. One should also note that all PAM constellation sets should be distinguishable from each other. The last $p_4^I = k \log_2(M^I)$ bits (modulation bits) are used to determine modulated symbols $\mathbf{s}^I = [s_1^I, \ldots, s_k^I]$, where modulated symbol s_v^I is generated from corresponding constellation set $S_{\psi_v}^I$ with $v \in \{1, \ldots, k\}$. Correspondingly, the transmitted signal vector $\mathbf{x}^I$ for the I-part can be expressed as

$$\mathbf{x}^I = \left[\sqrt{\frac{l_1^I}{I}} s_1^I, \sqrt{\frac{l_2^I}{I}} s_2^I, 0, \ldots, \sqrt{\frac{l_k^I}{I}} s_k^I, 0, \ldots, 0\right]^T. \quad (18)$$

For the Q-part with p^Q bits, the encoding procedure is symmetric, and another k among n subcarriers are activated for transmitting the imaginary part of transmitted signal. Similarly, p^Q bits are also split into four parts as $p^Q = p_1^Q + p_2^Q + p_3^Q + p_4^Q$. The $p_1^Q = \lfloor \log_2 C(n,k) \rfloor$ bits (index bits) are used to select SAP $\mathcal{I}^Q = \{i_1^Q, \ldots, i_k^Q\}$ with $\{i_\tau^Q\}_{\tau=1}^k \in \{1, 2, \ldots, n\}$. The $p_2^Q = \lfloor \log_2 C(I-1, k-1) \rfloor$ bits (composition bits) are utilized to determine EAP $\zeta^Q = \{l_1^Q, \ldots, l_k^Q\}$ with $\{l_\iota^Q\}_{\iota=1}^k \in \{1, 2, \ldots, I-1\}$ and $l_1^Q + \cdots + l_k^Q = I$, and the corresponding energy coefficients for the active subcarriers in the Q-part are given by $\{\sqrt{\frac{l_1^Q}{I}}, \ldots, \sqrt{\frac{l_k^Q}{I}}\}$. The $p_3^Q = \lfloor \log_2(k!) \rfloor$ bits (mode bits) are utilized to determine CAP $\chi^Q = \{\psi_1^Q, \ldots, \psi_k^Q\}$ with $\{\psi_v^Q\}_{v=1}^k \in \{1, 2, \ldots, k\}$ with respect to M^Q-ary PAM set $\{S_{\psi_1}^Q, \ldots, S_{\psi_k}^Q\}$. Similar to the PAM constellation sets for the I-part, all PAM constellation sets for the Q-part should also be distinguishable from each other. The last $p_4^Q = k \log_2(M^Q)$ bits (modulation bits) are used to determine modulated symbols $\mathbf{s}^Q = [s_1^Q, \ldots, s_k^Q]$, where the modulated symbol s_v^Q is generated from the corresponding constellation set $S_{\psi_v}^Q$ with $v \in \{1, \ldots, k\}$. Therefore, the transmitted signal vector $\mathbf{x}^Q$

© 2022 IEEE. Personal use is permitted, but republication/redistribution requires IEEE permission. See https://www.ieee.org/publications/rights/index.html for more information.
Authorized licensed use limited to: KAUST. Downloaded on November 10,2022 at 05:42:06 UTC from IEEE Xplore. Restrictions apply.

This article has been accepted for publication in IEEE Transactions on Wireless Communications. This is the author's version which has not been fully edited and content may change prior to final publication. Citation information: DOI 10.1109/TWC.2022.3220752

TABLE VII
MAPPING TABLE FOR C-MM-OFDM-IQ-IM WITH $n = 4$, $k = 2$, AND $I = 4$

index bits (p_1)	SAP	composite bits (p_2)	EAP	mode bits (p_3)	CAP
[00]	$\{1, 2\}$	[0]	$\{1, 3\}$	[0]	$\{1, 2\}$
[01]	$\{1, 3\}$	[1]	$\{3, 1\}$	[1]	$\{2, 1\}$
[10]	$\{1, 4\}$				
[11]	$\{2, 3\}$				

for the Q-part can be expressed as

$$\mathbf{x}^Q = \left[\sqrt{\frac{l_1^Q}{I}}s_1^Q, \sqrt{\frac{l_2^Q}{I}}s_2^Q, 0, \ldots, \sqrt{\frac{l_k^Q}{I}}s_k^Q, 0, \ldots, 0\right]^T. \quad (19)$$

Finally, the transmitted signal vector for C-MM-OFDM-IQ-IM is generated by combining two vectors in the in-phase and quadrature domains as $\mathbf{x} = \mathbf{x}^I + j\mathbf{x}^Q$. Accordingly, the SE of C-MM-OFDM-IQ-IM can be increased and given by

$$r_{\mathrm{IQ}} = \frac{2\lfloor \log_2(C(n,k)\rfloor + 2\lfloor \log_2 C(I-1,k-1)\rfloor}{n} + \frac{2\lfloor \log_2 k!\rfloor + k\log_2 M^I + k\log_2 M^Q}{n}. \quad (20)$$

For illustration purposes, we give an example for C-MM-OFDM-IQ-IM with $n = 4$, $k = 2$, $I = 4$, and $M^I = M^Q = 2$ (2PAM). Two distinguishable PAM constellation sets are given by $\{S_1 = [-3, 1], S_2 = [-1, 3]\}$. Assume that the information bits required to be transmitted are given by 011011110010, and the mapping relationship is given in Table VII. For the I-part with 011011, the first two bits 01 select SAP $\{1, 3\}$, and the second one bit 1 selects EAP $\{3, 1\}$ with the corresponding energy coefficients $\{\sqrt{\frac{3}{4}}, \sqrt{\frac{1}{4}}\}$. The third one bit 0 indicates CAP $\{1, 2\}$ with corresponding sets $\{S_1, S_2\}$, and the last two bits 11 generate two modulated symbols $[1, 3]$ from $\{S_1, S_2\}$. Therefore, the real part of the transmitted signal is $\mathbf{x}^I = [\sqrt{\frac{3}{4}}, 0, \frac{3}{2}, 0]^T$. Similarly for the Q-part with 110010, the first two bits 11 select SAP $\{2, 3\}$, and the second one bit 0 selects EAP $\{1, 3\}$ with the corresponding energy coefficients $\{\sqrt{\frac{1}{4}}, \sqrt{\frac{3}{4}}\}$. The third one bit 0 indicates CAP $\{1, 2\}$ with the corresponding sets $\{S_1, S_2\}$, and the last two bits 10 generate two modulated symbols $[1, -1]$ from $\{S_1, S_2\}$. Therefore, the imaginary part of the transmitted signal is $\mathbf{x}^Q = [0, \frac{1}{2}, -\sqrt{\frac{3}{4}}, 0]^T$. Finally, the transmitted signal vector (prior to normalization) is given by merging the two vectors in the in-phase and quadrature domains to be $\mathbf{x} = \mathbf{x}^I + j\mathbf{x}^Q = [\sqrt{\frac{3}{4}}, \frac{1}{2}j, \frac{3}{2} - j\sqrt{\frac{3}{4}}, 0]^T$.

With respect to C-MM-OFDM-IQ-IM-II, it can be observed from the above encoding procedure that the constructions of index bits, composite bits, and modulation bits for the I-part and Q-part are exactly the same as those in C-MM-OFDM-IQ-IM. The only difference for these two schemes is the construction of mode bits. In the I-part or Q-part of C-MM-OFDM-IQ-IM, only k distinguishable PAM sets are utilized, while Q distinguishable PAM sets are used for the I-part or Q-part of C-MM-OFDM-IQ-IM-II. By following the Q-ary code construction method given in Section II-C, the number of mode bits for the I-part (or Q-part) in C-MM-OFDM-IQ-IM-II is $\lfloor \log_2 Q^{k-1}\rfloor$, which results in the SE superiority over C-MM-OFDM-IM-II. From this reasoning, the SE of C-MM-OFDM-IQ-IM-II can be calculated as

$$r_{\mathrm{IQ-II}} = \frac{2\lfloor \log_2(C(n,k)\rfloor + 2\lfloor \log_2 C(I-1,k-1)\rfloor}{n} + \frac{2\lfloor \log_2 Q^{k-1}\rfloor + k\log_2 M^I + k\log_2 M^Q}{n}. \quad (21)$$

In addition, the low-complexity detection method and performance analysis for C-MM-OFDM-IM(-II) provided in Sections II and III are also applicable to GC-MM-OFDM-IM(-II) and C-MM-OFDM-IQ-IM(-II), due to the similar configurations of C-MM-OFDM-IM(-II), GC-MM-OFDM-IM(-II), and C-MM-OFDM-IQ-IM(-II). Therefore, we do not repeatedly describe the low-complexity detection method and performance analysis for GC-MM-OFDM-IM(-II) and C-MM-OFDM-IQ-IM(-II) in this section.

V. SIMULATION RESULTS

In this section, we illustrate the computer simulation results for numerically evaluating the BER performance of C-MM-OFDM-IM(-II), GC-MM-OFDM-IM(-II), and C-MM-OFDM-IQ-IM(-II) schemes under the assumptions of Rayleigh fading channels and perfect channel estimation. For convenience, we adopt the shorthands as follows:

- "OFDM, (n, MPSK/QAM)" denotes OFDM with n subcarriers and M-ary PSK/QAM constellation set.
- "OFDM-IM, (n, k, MPSK/QAM)" denotes OFDM-IM with n subcarriers, k active subcarriers, and M-ary PSK/QAM constellation set.
- "OFDM-ICM, (n, k, I, MPSK/QAM)" denotes OFDM-ICM with n subcarriers, k active subcarriers, total energy coefficient I, and M-ary PSK/QAM constellation set.
- "(G)C-MM-IM, (n, k, I, MPSK/QAM)" denotes (G)C-MM-OFDM-IM with n subcarriers, k active subcarriers, total energy coefficient I, and k distinguishable M-ary PSK/QAM constellation sets.
- "(G)C-MM-IM-II, (n, k, I, Q, MPSK/QAM)" denotes (G)C-MM-OFDM-IM-II with n subcarriers, k active subcarriers, total energy coefficient I, and Q distinguishable M-ary PSK/QAM constellation sets.
- "C-MM-IQ-IM, (n, k, I, M^IPAM, M^QPAM)" denotes C-MM-OFDM-IQ-IM with n subcarriers, k active subcarriers, total energy coefficient I, k distinguishable M^I-ary and M^Q-ary PAM constellation sets for I-part and Q-part, respectively.

© 2022 IEEE. Personal use is permitted, but republication/redistribution requires IEEE permission. See https://www.ieee.org/publications/rights/index.html for more information.
Authorized licensed use limited to: KAUST. Downloaded on November 10,2022 at 05:42:06 UTC from IEEE Xplore. Restrictions apply.

This article has been accepted for publication in IEEE Transactions on Wireless Communications. This is the author's version which has not been fully edited and content may change prior to final publication. Citation information: DOI 10.1109/TWC.2022.3220752

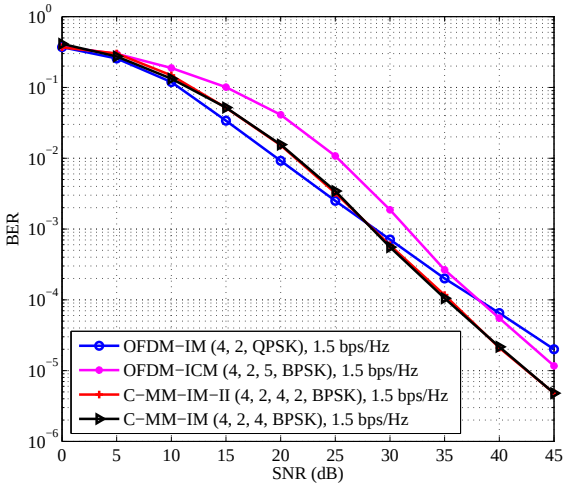


Fig. 3. BER comparison between OFDM-IM, OFDM-ICM, and C-MM-OFDM-IM(-II) with $n = 4$.

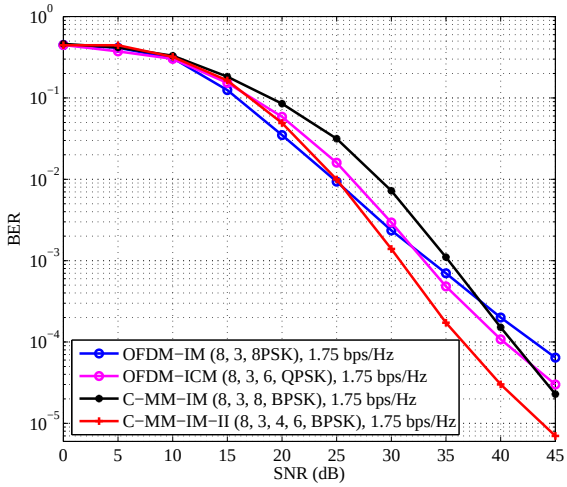


Fig. 4. BER comparison between OFDM-IM, OFDM-ICM, and C-MM-OFDM-IM with $n = 8$.

- "C-MM-IQ-IM-II, (n, k, I, Q, M^IPAM, M^QPAM)" denotes C-MM-OFDM-IQ-IM-II with n subcarriers, k active subcarriers, total energy coefficient I, Q distinguishable M^I-ary and M^Q-ary PAM constellation sets for I-part and Q-part, respectively.

In Fig. 3, we compare the BER performance of OFDM-IM, OFDM-ICM, C-MM-OFDM-IM, and C-MM-OFDM-IM-II with $n = 4$ and PSK under the SE of 1.5 bps/Hz. It can be seen from Fig. 3 that the proposed C-MM-OFDM-IM and C-MM-OFDM-IM-II schemes both achieve better BER performance than OFDM-IM and OFDM-ICM. Specifically, compared to "OFDM-ICM (4, 2, 5, BPSK)", "C-MM-IM (4, 2, 4, BPSK)" and "C-MM-IM-II (4, 2, 4, 2, BPSK)" both obtain better BER performance over the entire SNR region and achieve about 2 dB SNR gain in the high SNR region. Compared to "OFDM-IM (4, 2, QPSK)", "C-MM-IM (4, 2, 4, BPSK)" and "C-MM-IM-II (4, 2, 4, 2, BPSK)" obtain the worse BER performance in the low SNR region due to the erroneous estimation of EAP and CAP, while they obtain about 4 dB SNR gain in the high SNR region because of less estimation errors dominated by the BPSK modulation. In addition, we can see that "C-MM-IM (4, 2, 4, BPSK)" and "C-MM-IM-II (4, 2, 4, 2, BPSK)" have exactly the same BER performance with $Q = K = 2$, which verifies our hypothesis given in Section II-C.

To confirm our theoretical analysis and derivation, we further compare the BER performance of OFDM-IM, OFDM-ICM, C-MM-OFDM-IM, and C-MM-OFDM-IM-II with $n = 8$ under the SE of 1.75 bps/Hz in Fig. 4. From Fig. 4, we can still see that "C-MM-IM (8, 3, 8, BPSK)" and "C-MM-IM-II (8, 3, 4, 6, BPSK)" outperform and obtain about 2 dB and 6 dB SNR gain over "OFDM-IM (8, 3, 8PSK)", in the high SNR region. Moreover, "C-MM-IM-II (8, 3, 4, 6, BPSK)" outperforms "OFDM-ICM (8, 3, 6, QPSK)" over the entire SNR region with a constant 5 dB SNR gain for SNR $\geq$ 40 dB. Due to more EAP estimation errors, "C-MM-IM (8, 3, 8, BPSK)" is inferior to "OFDM-ICM (8, 3, 6, QPSK)" in the low SNR region, while obtaining better BER performance in the high SNR region, benefiting from the adopted BPSK modulation. This is because for most cases only the modulation estimation error exists in the high SNR region, whereas the estimation errors of SAP, EAP, and CAP dominate in the low SNR region but rarely happen in the high SNR region for C-MM-OFDM-IM(-II). It can also be observed that "C-MM-IM-II (8, 3, 4, 6, BPSK)" is superior to "C-MM-IM (8, 3, 8, BPSK)" with a 3 dB SNR gain in the high SNR region. This is because "C-MM-IM-II (8, 3, 4, 6, BPSK)" utilizes 2 EAPs for transmitting 1 composition bits ($I = 4$), while "C-MM-IM (8, 3, 8, BPSK)" utilizes 16 EAPs for transmitting 4 composition bits ($I = 8$), which leads to more EAP estimation errors over the entire SNR region.

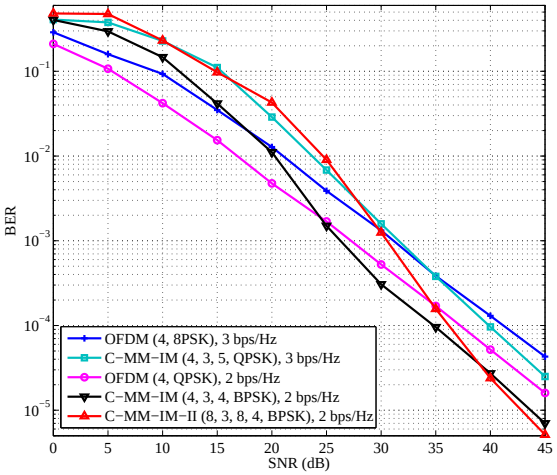


Fig. 5. Performance comparison of C-MM-OFDM-IM(-II) and OFDM with different configurations.

We compare the BER performance of C-MM-OFDM-IM(-II) and OFDM in Fig. 5. As shown in Fig. 5, we can see that "C-MM-IM, (4, 3, 5, QPSK)" with 3 bps/Hz achieves a lower

© 2022 IEEE. Personal use is permitted, but republication/redistribution requires IEEE permission. See https://www.ieee.org/publications/rights/index.html for more information.
Authorized licensed use limited to: KAUST. Downloaded on November 10,2022 at 05:42:06 UTC from IEEE Xplore. Restrictions apply.

This article has been accepted for publication in IEEE Transactions on Wireless Communications. This is the author's version which has not been fully edited and content may change prior to final publication. Citation information: DOI 10.1109/TWC.2022.3220752

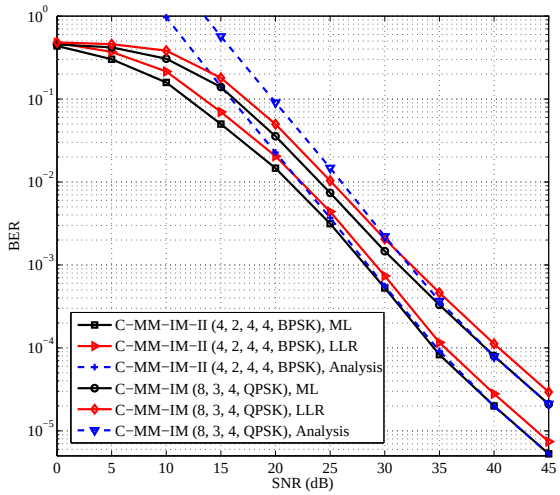


Fig. 6. BER comparison between the optimal ML detection and the proposed low-complexity LLR detection for C-MM-OFDM-IM(-II) with $n = 4$ and $n = 8$.

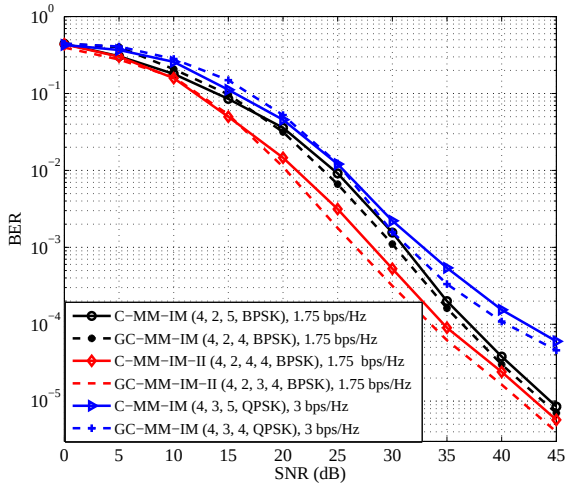


Fig. 7. BER comparison between (G)C-MM-OFDM-IM and (G)C-MM-OFDM-IM-II with $n = 4$.

BER with an about 1.5 dB SNR gain than "OFDM, (4, 8PSK)" with 3 bps/Hz in the high SNR region. In addition, we can also see that "C-MM-IM-II, (8, 3, 8, 4, BPSK)" and "C-MM-IM, (4, 3, 4, BPSK)" both with 2 bps/Hz still obtain up to a 4 dB SNR gain with respect to "OFDM, (4, QPSK)" with 2 bps/Hz in the high SNR region. Accordingly, the BER performance advantage of our proposed scheme is further substantiated.[1]

In Fig. 6, we compare the BER performance between the optimal ML detection with exponential computational complexity and the low-complexity detection for C-MM-OFDM-IM and C-MM-OFDM-IM-II with $n = 4$ and $n = 8$. As can be seen from the results depicted in Fig. 6 that the BER pertaining to the proposed low-complexity detection closely approaches the BER corresponding to the optimal ML detection with only a slight loss for C-MM-OFDM-IM(-II). Specifically, about 1 dB SNR loss appears between the low-complexity and ML detections for "C-MM-IM (8, 3, 4, QPSK)" and "C-MM-IM-II (4, 2, 4, 4, BPSK)", which is resulted from the misestimation on the SAP, EAP, and CAP by the LLR criterion. It can be still seen from Fig. 6 that the theoretical curves and simulation curves are well matched when SNR $\geq$ 40 dB, which confirms the accuracy of the upper-bounded BER analysis presented in Section III.[2]

Fig. 7 shows the BER performance of (G)C-MM-OFDM-IM and (G)C-MM-OFDM-IM-II with $n = 4$. We observe that GC-MM-OFDM-IM and GC-MM-OFDM-IM-II both outperform the corresponding C-MM-OFDM-IM and C-MM-OFDM-IM-II in the high SNR region. In particular "GC-MM-IM (4, 2, 4, BPSK)" with 1.75 bps/Hz obtains an almost 0.4 dB SNR gain over "C-MM-IM (4, 2, 5, BPSK)" with 1.75 bps/Hz in the high SNR region. Similarly, "GC-MM-IM-II (4, 2, 3, 4, BPSK)" with 1.75 bps/Hz achieves an almost 0.6 dB SNR gain over "C-MM-IM-II (4, 2, 4, 4, BPSK)" with 1.75 bps/Hz in the high SNR region. With SE increased to 1.75 bps/Hz, "GC-MM-IM (4, 3, 4, QPSK)" obtains an almost 1 dB SNR gain over "C-MM-IM (4, 3, 5, QPSK)" in the high SNR region. From above results, we can see that GC-MM-OFDM-IM(-II) is generally superior to C-MM-OFDM-IM(-II) with a significant performance gain, which stems from the less total energy coefficient I. Moreover, it is interesting that the performance gain can also be increased by increasing the modulation cardinality M and the number of active subcarriers k in the high SNR region. This is because GC-MM-OFDM-IM(-II) breaks the one-to-one mapping relationship, and its accuracy of estimation on modulation bits is higher than that of C-MM-OFDM-IM(-II) in the high SNR region.

In Fig. 8, we compare the BER performance of (G)C-MM-OFDM-IM and (G)C-MM-OFDM-IM-II with $n = 8$ under the same SE of 1.75 bps/Hz. It can be still seen that GC-MM-OFDM-IM(-II) obtains better BER performance than C-MM-OFDM-IM(-II) in the high SNR region. Similarly, "GC-MM-IM (8, 3, 6, BPSK)" and "GC-MM-IM-II (8, 3, 4, 4, BPSK)" both obtain almost a 0.6 dB SNR gain over "C-MM-IM (8, 3, 8, BPSK)" and "C-MM-IM-II (8, 3, 6, 4, BPSK)" in the high SNR region. This results further validates our hypothesis that the performance gain of GC-MM-OFDM-IM(-II) is attributed to a smaller total energy coefficient I. Meanwhile, it should be noticed from Figs. 7 and 8 that although the performance improvement between GC-MM-OFDM-IM(-II) and C-MM-OFDM-IM(-II) is not significant due to the limited SE increase (c.f., Table VI), GC-MM-OFDM-IM(-II) requires no additional frequency resource for such an improvement, which justifies its feasibility in practice.

To evaluate the BER performance of C-MM-OFDM-IQ-IM(-II), we conduct the computer simulations for C-MM-

[1]Note that the BER performance of the proposed scheme could be worse than the conventional OFDM and OFDM-IM schemes in the low SNR region. This is because the joint detection of index, composition, and mode bits is more prone to errors when the transmit power is not significantly greater than the noise power. Such a problem can be mitigated by introducing advanced coding techniques, which is out of the scope of this paper.

[2]The mismatch between the numerical and analytical results in the low SNR region is caused by the intrinsic principle of the union bound used for approximating the BER. The mismatch shall plummet with an increasing SNR, and, therefore, the analytical results at high SNR are accurate.

© 2022 IEEE. Personal use is permitted, but republication/redistribution requires IEEE permission. See https://www.ieee.org/publications/rights/index.html for more information.
Authorized licensed use limited to: KAUST. Downloaded on November 10,2022 at 05:42:06 UTC from IEEE Xplore. Restrictions apply.

This article has been accepted for publication in IEEE Transactions on Wireless Communications. This is the author's version which has not been fully edited and content may change prior to final publication. Citation information: DOI 10.1109/TWC.2022.3220752

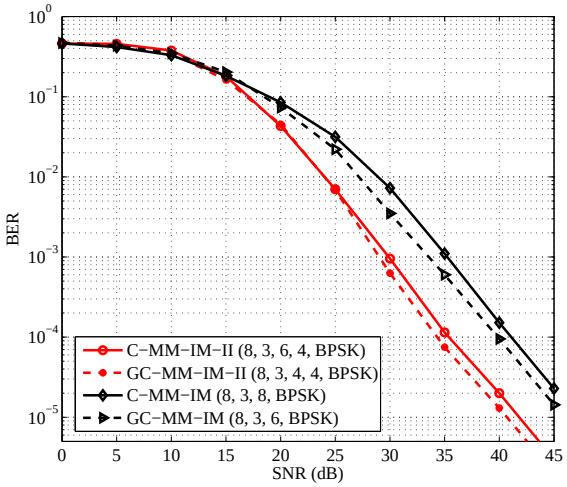


Fig. 8. BER comparison between (G)C-MM-OFDM-IM and (G)C-MM-OFDM-IM-II with $n = 8$.

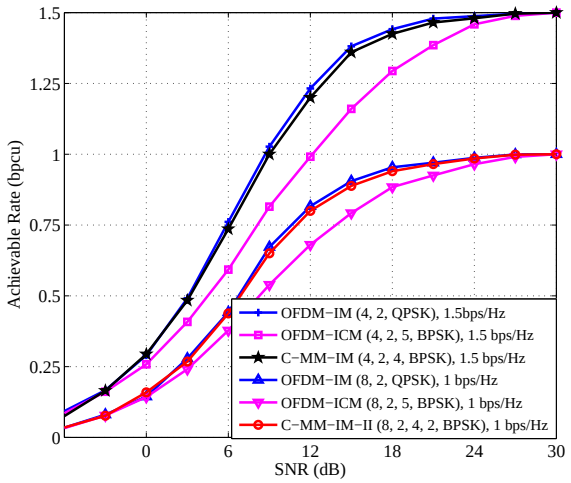


Fig. 10. Achievable rate comparison among C-MM-OFDM-IM(-II), OFDM-IM and OFDM-ICM schemes.

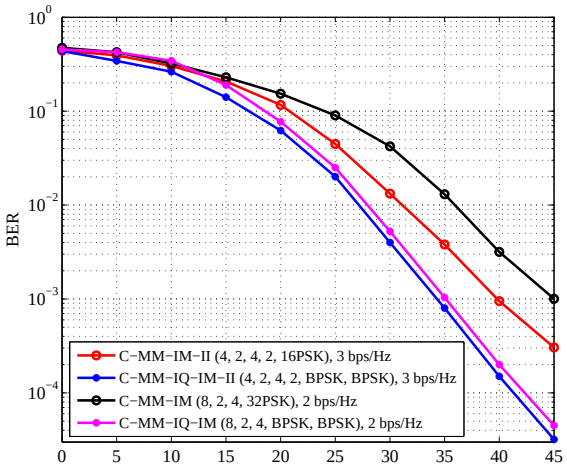


Fig. 9. BER comparison for C-MM-OFDM-IM(-II) and C-MM-OFDM-IQ-IM(-II).

OFDM-IM, C-MM-OFDM-IQ-IM, C-MM-OFDM-IM-II, and C-MM-OFDM-IQ-IM-II and present the simulation results in Fig. 9. Specifically, it can be seen that "C-MM-IQ-IM (8, 2, 4, 2PAM, 2PAM)" obtains almost a 10 dB SNR gain at BER$= 10^{-3}$ over "C-MM-IM (8, 2, 4, 32PSK)" under the same SE of 2 bps/Hz, where the significant performance improvement comes from the fact that C-MM-OFDM-IQ-IM adopts 2PAM with a low cardinality order, while C-MM-OFDM-IM employs 32PSK that causes the seriously degraded performance. We can also see that "C-MM-IQ-IM-II (4, 2, 4, 2, 2PAM, 2PAM)" outperforms "C-MM-IM-II (4, 2, 4, 2, 16PSK)" with a 7 dB SNR gain under the SE of 2 bps/Hz. This is also because of the 16PSK in C-MM-OFDM-IM-II, and C-MM-OFDM-IQ-IM-II is thus able to achieve the considerable performance enhancement. In summary, by lowering down the modulation order and extending the processing in both in-phase and quadrature constellation domains, C-MM-OFDM-IQ-IM-II is capable of improving SE in a large scale.

Additionally, Fig. 10 presents the achievable rates of OFDM-IM, OFDM-ICM, C-MM-OFDM-IM, and C-MM-OFDM-IM-II. From Fig. 10, we find that the achievable rates of all schemes increase with the increase of SNR and approach to constants in the high SNR region due to the rare error estimation as SNR increases. More importantly, although the achievable rates of all schemes tend to saturate at high SNR, the increment of achievable rates of "C-MM-IM (4, 2, 4, BPSK)" and "OFDM-IM (4, 2, QPSK)" both with SE of 1.5 bps/Hz are quite similar over the entire SNR region, and both are higher than "OFDM-ICM (4, 2, 5, BPSK)" with SE of 1.5 bps/Hz in the low-to-medium SNR region. The similar situation happens for "OFDM-IM (8, 2, QPSK)", "OFDM-ICM (8, 2, 5, BPSK)", and "C-MM-IM-II (8, 2, 4, 2, BPSK)" with SE of 1 bps/Hz. We also see that "OFDM-ICM (8, 2, 5, BPSK)" achieves the lowest increment of the achievable rate, and both "C-MM-IM-II (8, 2, 4, 2, BPSK)" and "OFDM-IM (8, 2, QPSK)" have a similar and higher increment of the achievable rate, which clearly reveals the advantage of our proposed schemes.

VI. Conclusions

In this paper, we proposed the C-MM-OFDM-IM(-II) scheme to overcome the drawbacks of the conventional OFDM-IM and OFDM-ICM schemes by simultaneously extending the indexing concept to the energy and constellation domains. An LLR based detection scheme for C-MM-OFDM-IM(-II) was proposed, which approaches the optimal ML detection with much less computational complexity. Moreover, the upper-bounded BER and lower-bounded achievable rate of C-MM-OFDM-IM(-II) were derived in closed form. In order to increase the SE of C-MM-OFDM-IM(-II), we further proposed two enhanced schemes, named GC-MM-OFDM-IM(-II) and C-MM-OFDM-IQ-IM(-II). Specifically, GC-MM-OFDM-IM(-II) breaks the one-to-one mapping and jointly utilizes all SAPs, EAPs, and CAPs for transmission purposes. C-MM-OFDM-IQ-IM(-II) extends the indexing concept to the in-phase and quadrature constellation domains. Finally, computer

© 2022 IEEE. Personal use is permitted, but republication/redistribution requires IEEE permission. See https://www.ieee.org/publications/rights/index.html for more information.
Authorized licensed use limited to: KAUST. Downloaded on November 10,2022 at 05:42:06 UTC from IEEE Xplore. Restrictions apply.

This article has been accepted for publication in IEEE Transactions on Wireless Communications. This is the author's version which has not been fully edited and content may change prior to final publication. Citation information: DOI 10.1109/TWC.2022.3220752

simulations showed that C-MM-OFDM-IM(-II) is superior to OFDM-IM and OFDM-ICM under the same SE requirement. They also showed that GC-MM-OFDM-IM(-II) and C-MM-OFDM-IQ-IM(-II) outperform C-MM-OFDM-IM(-II) in the high SNR region.

REFERENCES

[1] S. Dang, O. Amin, B. Shihada, and M.-S. Alouini, "What should 6G be?," *Nature Electronics*, vol. 3, pp. 20-29, Jan. 2020.

[2] E. Basar, M. Wen, R. Mesleh, M. Di Renzo, Y. Xiao, and H. Haas, "Index modulation techniques for next-generation wireless networks," *IEEE Access*, vol. 5, pp. 16693-16746, 2017.

[3] M. Wen *et al.*, "A survey on spatial modulation in emerging wireless systems: Research progresses and applications," *IEEE J. Sel. Areas Commun.*, vol. 37, no. 9, pp. 1949-1972, Sept. 2019.

[4] N. Ishikawa, S. Sugiura, and L. Hanzo, "50 years of permutation, spatial and index modulation: From classic RF to visible light communications and data storage," *IEEE Commun. Surveys Tuts.*, vol. 20, No. 3, pp. 1905-1938, 3rd Quart., 2018.

[5] T. Mao, Q. Wang, Z. Wang, and S. Chen, "Novel index modulation techniques: A survey," *IEEE Commun. Surveys Tuts.*, vol. 21, no. 1, pp. 315-348, 1st Quart., 2019.

[6] R. Mesleh, *et al.*, "Spatial modulation," *IEEE Trans. Veh. Technol*., vol. 57, no. 4, pp. 2228-2241, July 2008.

[7] J. Jeganathan, A. Ghrayeb, L. Szczecinski, and A. Ceron, "Space shift keying modulation for MIMO channels," *IEEE Trans. Wireless Commun.*, vol. 8, no. 7, pp. 3692-3703, July 2009.

[8] A. Younis, N. Serafimovski, R. Mesleh, and H. Haas, "Generalised spatial modulation," in *Proc. 2010 Conf. Record of the 44th Asilomar Conf. on Signals, Syst. and Comput.*, Pacific Grove, CA, USA, Nov. 2010, pp. 1498-1502.

[9] J. Jeganathan, A. Ghrayeb, and L. Szczecinski, "Generalized space shift keying modulation for MIMO channels," in *Proc. IEEE 19th Int. Symp. PIMRC*, Cannes, France, Sept. 2008, pp. 1-5.

[10] R. Mesleh *et al.*, "Quadrature spatial modulation," *IEEE Trans. Veh. Technol.*, vol. 64, no. 6, pp. 2738-2742, June 2015.

[11] J. Li *et al.*, "Generalized quadrature spatial modulation and its application to vehicular networks with NOMA," *IEEE Trans. Intell. Transp. Syst.*, vol. 66, no. 2, pp. 4030-4039, July 2021.

[12] S. Sugiura, S. Chen, and L. Hanzo, "Generalized space-time shift keying designed for flexible diversity-, multiplexing- and complexity-tradeoffs," *IEEE Trans. Wireless Commun.*, vol. 10, no. 4, pp. 1144-1153, Apr. 2011.

[13] E. Basar, U. Aygolu, E. Panayirci, and H. Poor, "Space-time block coded spatial modulation," *IEEE Trans. Commun.*, vol. 59, no. 3, pp. 823-832, Mar. 2011.

[14] X.-Q. Jiang, H. Hai, J. Hou, J. Li, and W. Duan, "Euclidean geometries based space-time block coded spatial modulation," *IEEE J. Selected Topics Signal Process.*, vol. 13, no. 6, pp. 1301-1311, Oct. 2019.

[15] Y. Bian *et al.*, "Differential spatial modulation," *IEEE Trans. Veh. Technol.*, vol. 64, no. 7, pp. 3262-3268, July 2015.

[16] L. Yang, "Transmitter preprocessing aided spatial modulation for multiple-input multiple-output systems," in *Proc. of 73rd IEEE Veh. Techn. Conf. (VTC Spring)*, Budapest, Hungary, May 2011, pp. 1-5.

[17] R. Zhang, L. Yang, and L. Hanzo, "Generalised pre-coding aided spatial modulation," *IEEE Trans. Wireless Commun.*, vol. 12, no. 11, pp. 5434-5443, Nov. 2013.

[18] A. Stavridis *et al.*, "Performance analysis of multi-stream receive spatial modulation in the MIMO broadcast channel," *IEEE Trans. Wireless Commun.*, vol. 15, no. 3, pp. 1808-1820, Mar. 2016.

[19] J. Li, M. Wen, X. Cheng, Y. Yan, S. Song, and M. H. Lee, "Generalised pre-coding aided quadrature spatial modulation," *IEEE Trans. Veh. Technol.*, vol. 66, no. 2, pp. 1881-1886, Feb. 2017.

[20] E. Basar, U. Aygolu, E. Panayirci, and H. V. Poor, "Orthogonal frequency division multiplexing with index modulation," *IEEE Trans. Signal Process.*, vol. 61, no. 22, pp. 5536-5549, Nov. 2013.

[21] M. Wen, Y. Zhang, J. Li, E. Basar, and F. Chen, "Equiprobable subcarrier activation method for OFDM with index modulation," *IEEE Commun. Lett.*, vol. 20, no. 12 pp. 2386-2389, Dec. 2016.

[22] Y. Xiao, S. Wang, L. Dan, X. Lei, P. Yang, and W. Xiang, "OFDM with interleaved subcarrier-index modulation," *IEEE Commun. Lett.*, vol. 18, no. 8, pp. 1447-1450, Aug. 2014.

[23] M. Wen, B. Ye, E. Basar, Q. Li, and F. Ji, "Enhanced orthogonal frequency division multiplexing with index modulation," *IEEE Trans. Wireless Commun.*, vol. 16, no. 7, pp. 4786-4801, July 2017.

[24] A. I. Siddiq, "Low complexity OFDM-IM detector by encoding all possible subcarrier activation patterns," *IEEE Commun. Lett.*, vol. 20, no. 3, pp. 446-449, Mar. 2016.

[25] R. Fan, Y. J. Yu, and Y. L. Guan, "Generalization of orthogonal frequency division multiplexing with index modulation," *IEEE Trans. Wireless Commun.*, vol. 14, no. 10, pp. 5350-5359, Oct. 2015.

[26] J. Li, S. Dang, M. Wen, X.-Q. Jiang, Y. Peng, and H. Hai, "Layered orthogonal frequency division multiplexing with index modulation," *IEEE Syst. J.*, vol. 13, no. 4, pp. 3793-3802, Dec. 2019.

[27] F. Yarkin and J. P. Coon, "Index and composition modulation," *IEEE Commun. Lett.*, vol. 25, no. 3, pp. 911-915, 2021.

[28] E. Basar, "On multiple-input multiple-output OFDM with index modulation for next generation wireless networks," *IEEE Trans. Signal Process.*, vol. 64, no. 15, pp. 3868-3878, Aug. 2016.

[29] T. Mao *et al.*, "Dual-mode index modulation aided OFDM," *IEEE Access*, vol. 5, pp. 50-60, 2017.

[30] T. Mao, Q. Wang, and Z. Wang, "Generalized dual-mode index modulation aided OFDM," *IEEE Commun. Lett.*, vol. 21, no. 4, pp. 761-764, Apr. 2017.

[31] M. Wen, E. Basar, Q. Li, B. Zheng, and M. Zhang, "Multiple-mode orthogonal frequency division multiplexing with index modulation," *IEEE Trans. Commun.*, vol. 65, no. 9, pp. 3892-3906, Sep. 2017.

[32] F. Yarkin and J. P. Coon, "Q-ary multi-mode OFDM with index modulation," *IEEE Wireless Commun. Lett.*, vol. 9, no. 7, pp. 1110-1114, July 2020.

[33] M. Wen, Q. Li, E. Basar, and W. Zhang, "Generalized multiple-mode OFDM with index modulation," *IEEE Trans. Wireless Commun.*, vol. 17, no. 10, pp. 6531-6543, Oct. 2018.

[34] F. Yarkin *et al.*, "Set partition modulation," *IEEE Trans. Wireless Commun.*, vol. 19, no. 11, pp. 7557-7570, Nov. 2020.

[35] F. Yarkin and J. P. Coon, "Modulation based on a simple MDS code: Achieving better error performance than index modulation and related schemes," *IEEE Trans. Commun.*, vol. 70, no. 1, pp. 118-131, Jan. 2022.

[36] X. Cheng, M. Wen, L. Yang, and Y. Li, "Index modulated OFDM with interleaved grouping for V2X communications," in *Proc. IEEE Int. Conf. Intell. Transp. Syst. (ITSC)*, Qingdao, China, Oct. 2014, pp. 1097-1104.

[37] J. Li, Y. Peng, Y. Yan, X.-Q. Jiang, H. Hai and M. Zukerman, "Cognitive radio network assisted by OFDM with index modulation," *IEEE Trans. Veh. Technol.*, vol. 69, no. 1, pp. 1106-1110, Jan. 2020.

[38] J. Crawford, E. Chatziantoniou, and Y. Ko, "On the SEP analysis of OFDM index modulation with hybrid low complexity greedy detection and diversity reception," *IEEE Trans. Veh. Technol.*, vol. 66, no. 9, pp. 8103-8118, Sep. 2017.

[39] B. Zheng, M. Wen, E. Basar, and F. Chen, "Multiple-input multiple-output OFDM with index modulation: Low-complexity detector design," *IEEE Trans. Signal Process.*, vol. 65, no. 11, pp. 2758-2772, June 2017.

[40] J. Li, Q. Li, S. Dang, M. Wen, X.-Q. Jiang, and Y. Peng, "Low-complexity detection for index modulation multiple access," *IEEE Wireless Commun. Lett.*, vol. 9, no. 7, pp. 943-947, July 2020.

[41] R. Singleton, "Maximum distance Q-nary codes," *IEEE Trans. Inf. Theory*, vol. 10, no. 2, pp. 116-118, Apr. 1964.

[42] M. Chiani and D. Dardari, "Improved exponential bounds and approximation for the Q-function with application to average error probability computation," in *Proc. IEEE Global Telecommun. Conf.*, Bologna, Italy, 2002, pp. 1399-1402.

[43] J. G. Proakis, *Digital Communications*, 3rd ed. New York: McGraw-Hill, 1995.

[44] M. Wen, X. Cheng, M. Ma, B. Jiao, and H. V. Poor, "On the achievable rate of OFDM with index modulation," *IEEE Trans. Signal Process.*, vol. 64, no. 8, pp. 1919-1932, Apr. 2016.



Jun Li (Member, IEEE) received the Ph.D. degrees from Chonbuk National University, Jeonju, South Korea, in 2016. He is currently an Associate Professor with Guangzhou University, Guangzhou, China. He has published more than 60 papers in refereed journals and conference proceedings. His research interests include spatial modulation, OFDM with index modulation, and reconfigurable intelligent surface.

© 2022 IEEE. Personal use is permitted, but republication/redistribution requires IEEE permission. See https://www.ieee.org/publications/rights/index.html for more information.
Authorized licensed use limited to: KAUST. Downloaded on November 10,2022 at 05:42:06 UTC from IEEE Xplore. Restrictions apply.

This article has been accepted for publication in IEEE Transactions on Wireless Communications. This is the author's version which has not been fully edited and content may change prior to final publication. Citation information: DOI 10.1109/TWC.2022.3220752



Shuping Dang (Member, IEEE) received B.Eng (Hons) in Electrical and Electronic Engineering from the University of Manchester (with first class honors) and B.Eng in Electrical Engineering and Automation from Beijing Jiaotong University in 2014 via a joint '2+2' dual-degree program. He also received D.Phil in Engineering Science from University of Oxford in 2018. Dr. Dang worked as a Postdoctoral Fellow with the Computer, Electrical and Mathematical Science and Engineering Division, King Abdullah University of Science and Technology (KAUST). Dr. Dang joined in the R&D Center, Huanan Communication Co., Ltd. after graduating from University of Oxford and worked as a Postdoctoral Fellow with the Computer, Electrical and Mathematical Science and Engineering Division, King Abdullah University of Science and Technology (KAUST). He is currently a Lecturer with Department of Electrical and Electronic Engineering, University of Bristol. The research interests of Dr. Dang include 6G communications, wireless communications, wireless security, and machine learning for communications.



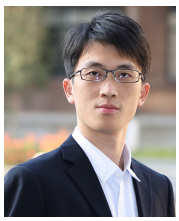
Yu Huang received the Ph.D. degree from South China University of Technology, Guangzhou, China. He is currently an Associate Professor with Guangzhou University, Guangzhou, China. His main research interests include molecular communications and wireless communications. He was the winner of the Data Bakeoff Competition (Molecular MIMO) at the IEEE Communication Theory Workshop held in Selfoss, Iceland, in 2019.



Pengxu Chen is a senior student and pursuing the B. S. degree in Guangzhou University, Guangzhou, China. He is currently working as an intern (algorithm engineer) in Shenzhen, China. His current research interests include index modulation, deep learning, and computer vision.



Xiaomin Qi received the B.S. degree from Central South University, Changsha, China, in 2018. She received the M.S. degree from South China University of Technology, Guangzhou, China, in 2022. Her current research interests include index modulation and NOMA.



Miaowen Wen (SM'18) received the Ph.D. degree from Peking University, Beijing, China, in 2014. From 2019 to 2021, he was with the Department of Electrical and Electronic Engineering, The University of Hong Kong, Hong Kong, as a Post-Doctoral Research Fellow. He is currently a Professor with South China University of Technology, Guangzhou, China. He has published two books and more than 160 journal papers. His research interests include a variety of topics in the areas of wireless and molecular communications.

Dr. Wen was a recipient of the IEEE Asia-Pacific (AP) Outstanding Young Researcher Award in 2020, and four Best Paper Awards from the IEEE ITST'12, the IEEE ITSC'14, the IEEE ICNC'16, and the IEEE ICCT'19. He was the winner in data bakeoff competition (Molecular MIMO) at IEEE Communication Theory Workshop (CTW) 2019, Selfoss, Iceland. He served as a Guest Editor for the IEEE JOURNAL ON SELECTED AREAS IN COMMUNICATIONS and for the IEEE JOURNAL OF SELECTED TOPICS IN SIGNAL PROCESSING. Currently, he is serving as an Editor for the IEEE TRANSACTIONS ON COMMUNICATIONS, the IEEE TRANSACTIONS ON MOLECULAR, BIOLOGICAL, AND MULTI-SCALE COMMUNICATIONS, and the IEEE COMMUNICATIONS LETTERS.



Huseyin Arslan (IEEE Fellow, IEEE Distinguished Lecturer, Member of Turkish Academy of Science) received his BS degree from the Middle East Technical University (METU), Ankara, Turkey in 1992; his MS and Ph.D. degrees were received respectively in 1994 and 1998 from Southern Methodist University (SMU), Dallas, TX. From January 1998 to August 2002, he was with the research group of Ericsson, where he was involved with several projects related to 2G and 3G wireless communication systems. Between August 2002 and August 2022, he was with the Electrical Engineering Department, at the University of South Florida, where he was a Professor. In December 2013, he joined Istanbul Medipol University to found the Engineering College, where he has been working as the Dean of the School of Engineering and Natural Sciences. In addition, he has worked as a part-time consultant for various companies and institutions including Anritsu Company, Savronik Inc., and The Scientific and Technological Research Council of Turkey. Dr. Arslan served as the founding Chairman of The Board Of Directors of ULAK Communication company, which is the Turkish telecom equipment provider. He was also the member of the Tubitak Scientific Board. Since May 2021, he is serving as a Member of the Board of Directors for Turkcell, the biggest cellular operator in Turkey while also operating in Ukrain, Belarus, and Cyprus.

Dr. Arslan conducts research in wireless systems, with emphasis on the physical and medium access layers of communications. His current research interests are on 6G and beyond radio access technologies, physical layer security, interference management (avoidance, awareness, and cancellation), cognitive radio, multi-carrier wireless technologies (beyond OFDM), dynamic spectrum access, co-existence issues, non-terrestial communications (High Altitude Platforms), joint radar (sensing) and communication designs. Dr. Arslan has been collaborating extensively with key national and international industrial partners and his research has generated significant interest in companies such as InterDigital, Anritsu, NTT DoCoMo, Raytheon, Honeywell, Keysight technologies. Collaborations and feedback from industry partners has significantly influenced his research. In addition to his research activities, Dr. Arslan has also contributed to wireless communication education. He has integrated the outcomes of his research into education which lead him to develop a number of courses at the University of South Florida and Istanbul Medipol University. He has developed a unique "Wireless Systems Laboratory" course (funded by the National Science Foundation and Keysight technologies) where he was able to teach not only the theory but also the practical aspects of wireless communication system with the most contemporary test and measurement equipment.

Dr. Arslan has served as general chair, technical program committee chair, session and symposium organizer, workshop chair, and technical program committee member in several IEEE conferences. He is currently a member of the editorial board for the IEEE Surveys and Tutorials and the Sensors Journal. He has also served as a member of the editorial board for the IEEE Transactions on Communications, the IEEE Transactions on Cognitive Communications and Networking (TCCN), and several other scholarly journals by Elsevier, Hindawi, and Wiley Publishing.

© 2022 IEEE. Personal use is permitted, but republication/redistribution requires IEEE permission. See https://www.ieee.org/publications/rights/index.html for more information.
Authorized licensed use limited to: KAUST. Downloaded on November 10,2022 at 05:42:06 UTC from IEEE Xplore. Restrictions apply.